

Statistics of Giant Radio Halos from Electron Reacceleration Models

R. Cassano,^{1,2*} G. Brunetti², G. Setti^{1,2}

¹ *Dipartimento di Astronomia, Università di Bologna, via Ranzani 1, I-40127 Bologna, Italy*

² *Istituto di Radioastronomia - INAF, via Gobetti 101, I-40129 Bologna, Italy*

5 February 2008

ABSTRACT

The most important evidence of non-thermal phenomena in galaxy clusters comes from Giant Radio Halos (GRHs), spectacular synchrotron radio sources extended over \geq Mpc scales, detected in the central regions of a growing number of massive galaxy clusters. A promising possibility to explain these sources is given by *in situ* stochastic reacceleration of relativistic electrons by turbulence generated in the cluster volume during merger events. Cassano & Brunetti (2005) have recently shown that the expected fraction of clusters with radio halos and the increase of such a fraction with cluster mass can be reconciled with present observations provided that a fraction of 20-30 % of the turbulence in clusters is in the form of compressible modes.

In this work we extend the above mentioned analysis, by including a scaling of the magnetic field strength with cluster mass. We show that, in the framework of the reacceleration model, the observed correlations between the synchrotron radio power of a sample of 17 GRHs and the X-ray properties of the hosting clusters are consistent with, and actually predicted by a magnetic field dependence on the virial mass of the form $B \propto M_v^b$, with $b \gtrsim 0.5$ and typical μ G strengths of the average B intensity. The occurrence of GRHs as a function of both cluster mass and redshift is obtained: the evolution of such a probability depends on the interplay between synchrotron and inverse Compton losses in the emitting volume, and it is maximized in clusters for which the two losses are comparable.

The most relevant findings are that the predicted luminosity functions of GRHs are peaked around a power $P_{1.4\text{GHz}} \sim 10^{24}$ W/Hz, and severely cut-off at low radio powers due to the decrease of the electron reacceleration in smaller galaxy clusters, and that the occurrence of GRHs at 1.4 GHz beyond a redshift $z \sim 0.7$ appears to be negligible. As a related check we also show that the predicted integral radio source counts within a limited volume ($z \leq 0.2$) are consistent with present observational constraints. Extending the source counts beyond $z=0.2$ we estimate that the total number of GRHs to be discovered at \sim mJy radio fluxes could be ~ 100 at 1.4 GHz. Finally, the occurrence of GRHs and their number counts at 150 MHz are estimated in view of the forthcoming operation of low frequency observatories (LOFAR, LWA) and compared with those at higher radio frequencies.

Key words: particle acceleration - turbulence - radiation mechanisms: non-thermal - galaxies: clusters: general - radio continuum: general - X-rays: general

1 INTRODUCTION

The intracluster medium (ICM) is a mixture of thermal and non-thermal components and a precise physical description

of the ICM also requires adequate knowledge of the role of non-thermal components.

The most detailed evidence for non-thermal phenomena comes from the radio observations. A number of clusters of galaxies are known to contain wide diffuse synchrotron sources (radio halos and relics) which have no obvious connection with the individual cluster galaxies, but are rather

* E-mail: rcassano@ira.inaf.it

associated to the ICM (e.g., Giovannini & Feretti 2000; Kempner & Sarazin 2001; see Giovannini & Feretti 2002 for a review). The synchrotron emission of such sources requires a population of GeV relativistic electrons (and/or positrons) and cluster magnetic fields on μG levels. Evidence for relativistic electrons (and positrons) in the ICM may also come from the detection of hard X-ray (HXR) excess emission in the case of a few galaxy clusters (e.g., Rephaeli & Gruber 2003, Fusco-Femiano et al. 2004), and possibly from extreme ultra-violet (EUV) excess emission (e.g., Kaastra et al. 2003; Bowyer et al. 2004). It is also believed that the amount of the energy budget of high energy protons in the ICM might be significant, due to the confinement of cosmic rays over cosmological time scales (Völk et al. 1996; Berezhinsky, Blasi & Ptuskin 1997; Enßlin et al. 1997). Nevertheless, the gamma radiation that would allow to infer the fraction of relativistic hadrons in clusters has not been detected as yet (Reimer et al., 2003, see Pfrommer & Enßlin 2004 for upper limit on this fraction).

Shock waves are unavoidably formed during merger events; they may efficiently accelerate relativistic particles contributing to the injection of relativistic hadrons and of relativistic emitting electrons in the ICM (e.g., Ryu et al. 2003, Gabici & Blasi 2003). However the accelerated electrons have a short pathlength due to IC losses and thus they can travel a short distance away from the shock front, emitting synchrotron radiation concentrated around the shock rim (e.g., Miniati et al. 2001). Radio Relics, which are polarized and elongated radio sources located in the cluster peripheral regions, may indeed be associated to these shock waves, as a result of Fermi-I diffusive shock acceleration of ICM electrons (Enßlin et al. 1998; Roettiger et al. 1999), or of adiabatic energization of relativistic electrons confined in fossil radio plasma, released in the past by active radio galaxies (Enßlin & Gopal-Krishna 2001; Hoeft et al. 2004).

The most spectacular evidence of diffuse synchrotron emission in galaxy clusters is that associated to giant radio halos, Mpc-size radio sources which permeate the cluster volume similarly to the X-ray emitting gas. In this respect, two main possibilities have been investigated in some detail to explain that GeV electrons (and/or positrons) are present and able to radiate on distance scales larger than their typical loss lengths: *i*) the so-called *reacceleration* models, whereby relativistic electrons (and positrons) injected in the ICM by a variety of processes active during the life of galaxy clusters are continuously re-energized *in situ* during the life-time of the observed radio halos (which is estimated to be ~ 1 Gyr, Kuo et al. 2004) and *ii*) the *secondary electron* models, whereby electrons are secondary products of the hadronic interactions of cosmic rays with the intracluster medium, as first proposed by Dennison (1980). Although the origin of the emitting particles in radio halos is still a matter of debate (e.g., Enßlin 2004), the above two models for the production of the radiating electrons (and positrons) have a substantial predictive power, which can be used to discriminate among such models by comparing their predictions with observations. Although future observations remain crucial to achieve a firm conclusion, at least as far as the few well studied clusters and the analysis of statistical samples are concerned, present data seem to suggest the presence of *in situ* particle-reacceleration mechanisms ac-

tive in the ICM (e.g., Brunetti 2003,04; Blasi 2004; Feretti et al. 2004; Hwang 2004; Reimer et al. 2004).

Radio observations of galaxy clusters indicate that the detection rate of radio halos shows an abrupt increase with increasing the X-ray luminosity of the host clusters. In particular, about 30-35% of the galaxy clusters with X-ray luminosity larger than 10^{45} erg/s show diffuse non-thermal radio emission (Giovannini & Feretti 2002); these clusters have also high temperature ($kT > 7$ keV) and large mass ($\gtrsim 2 \times 10^{15} M_{\odot}$). Furthermore, giant radio halos are always found in merging clusters (e.g., Buote 2001; Schuecker et al. 2001). Although the physics of particle acceleration due to turbulence generated in merging clusters has been investigated in some detail (e.g., Schlickeiser et al. 1987; Petrosian 2001; Fujita et al. 2003; Brunetti et al. 2004; Brunetti & Blasi 2005) and the model expectations seem to reproduce the observed radio features and possibly also the hard X-rays (e.g., Brunetti et al. 2001; Kuo et al. 2003; Brunetti 2004; Hwang 2004), a theoretical investigation of the statistical properties of the Mpc diffuse emission in galaxy clusters in the framework of these models has not been carried out extensively as yet. In particular, the fact that giant radio halos are always associated to massive galaxy clusters and the presence of a trend between their radio power and the mass (temperature, X-ray luminosity) of the parent clusters may be powerful tools to test and constrain present models.

In a recent paper Cassano & Brunetti (2005; hereafter CB05) have modelled the statistical properties of giant radio halos in the framework of the merger-induced *in situ* particle acceleration scenario. By adopting the semi-analytic Press & Schechter (1974; PS74) theory to follow the cosmic evolution and formation of a large synthetic population of galaxy clusters, it was assumed that the energy injected in the form of magnetosonic waves during merging events in clusters is a fraction, η_t , of the PdV work done by the infalling subclusters in passing through the most massive one. Then the processes of stochastic acceleration of the relativistic electrons by these waves, and the ensuing synchrotron emission properties, have been worked out under the assumption that the magnetic field intensities, ICM temperatures and particle densities (both thermal and non-thermal) have constant volume averaged values (within 1 Mpc^3). The main findings of these calculations is that giant radio halos are *naturally* expected only in the more massive clusters, and the expected fraction of clusters with radio halos (at redshifts $z \lesssim 0.2$) can be reconciled with the observed one under viable assumptions ($\eta_t \simeq 0.24 - 0.34$). Specifically, the probability to form giant radio halos in the synthetic cluster population was found to be of order 20-30 % in the more massive galaxy clusters ($M > 2 \times 10^{15} M_{\odot}$), 2-5 % in $M \sim 10^{15} M_{\odot}$ clusters, and negligible in less massive systems. Such increase of the probability with the cluster mass is essentially due to the increase of both the energy density of turbulence and of the turbulence injection volume with cluster mass (see CB05).

The present paper is a natural extension of the CB05 work, the most important difference being that here we adopt a scaling law between the rms magnetic field strength (averaged in the synchrotron emitting volume) and the virial mass of the parent clusters, $B \propto M^b$. We carry out a detailed comparison between statistical data of giant radio halos currently available and model expectations as derived by adopting the CB05 procedures.

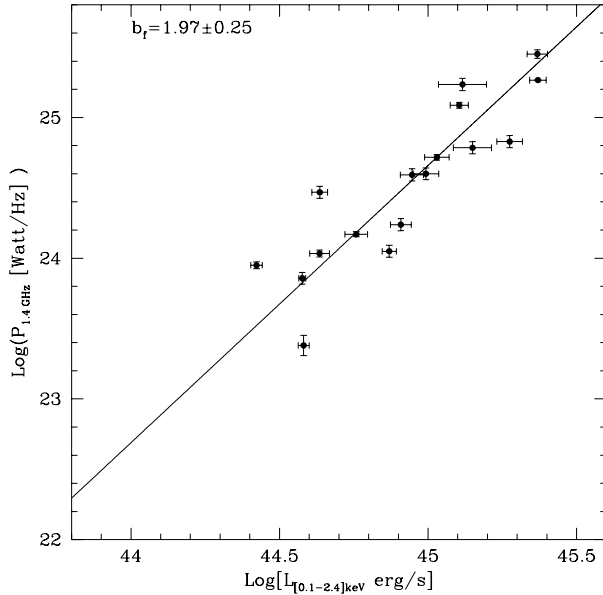


Figure 1. Correlation between the radio power at 1.4 GHz and the X-ray luminosity between [0.1-2.4] keV for the GRHs.

In Sec. 2 we collect radio and X-ray data for well known giant radio halos from the literature and derive radio–X-ray correlations. In Sec. 3 we investigate the possibility to match the observed radio–X-ray correlations for giant radio halos with electron acceleration models. This comparison provides stringent constraints on the physical parameters in the ICM, in particular for the magnetic field in galaxy clusters. In Sec. 4 we derive the expected probability to form giant radio halos as a function of M_v and z . This is done by adopting the same values of the physical parameters which allows to account for the observed radio–X-ray correlations. In Secs. 5–6 we finally calculate the expected luminosity functions and number counts of giant radio halos.

As in CB05, we focus our attention on giant radio halos only (linear size $\sim 1 h_{50}^{-1}$ Mpc, GRHs elsewhere). The adopted cosmology is: Λ CDM ($H_0 = 70 \text{ Km s}^{-1} \text{ Mpc}^{-1}$, $\Omega_{o,m} = 0.3$, $\Omega_\Lambda = 0.7$, $\sigma_8 = 0.9$).

2 OBSERVED CORRELATIONS

In this section we discuss the observed correlations between the X-ray and the radio properties of clusters hosting GRHs. We collect galaxy clusters with known GRHs from the literature obtaining a total sample of 17 clusters. In Tab. 1 we report the radio and X-ray properties of this sample in a Λ CDM cosmology. In order to have the best estimate of the X-ray temperatures we select results from XMM-Newton observations when available, otherwise we use ASCA results or combine ASCA and Chandra information. We investigate the correlations between the X-ray and the radio properties of the selected clusters by making use of a linear regression fit in log-log space following the procedures given in Akritas & Bershadsky (1996). This method allows for intrinsic scatter and errors in both variables.

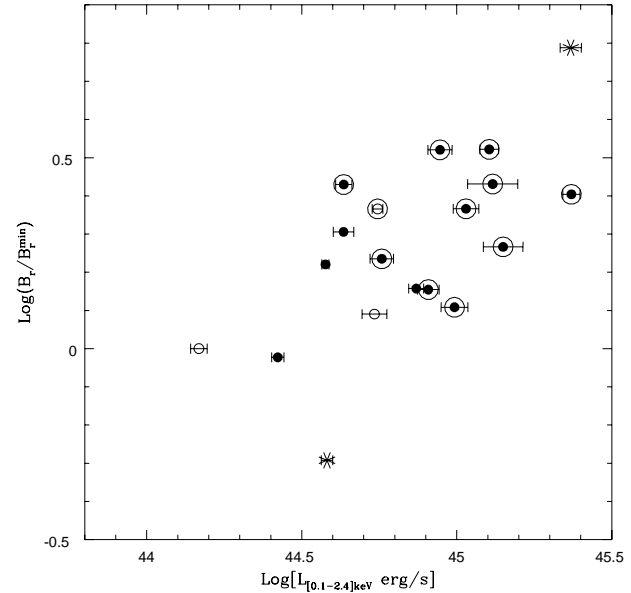


Figure 2. Halo radio brightness at 1.4 GHz, normalized to the radio brightness of A3562 (which is just visible in the NVSS), versus X-ray luminosity between [0.1-2.4] keV. Different symbols indicate GRHs (filled circles) and smaller radio halos (open circles) visible in the NVSS. Asterisks mark A2256, which falls below the NVSS surface brightness limit, and 1E50657-558, which falls below the declination range of the NVSS. Large circles mark objects visible in the NVSS and in the redshift range $z \sim 0.15 - 0.3$.

2.1 Radio Power–X-ray luminosity correlation

The presence of a correlation between the radio powers and the X-ray luminosities is well known (Liang et al. 2000; Feretti 2000, 2003; Enßlin and Röttgering 2002).

In Fig.1 we report the correlation between the X-ray luminosity (in the 0.1-2.4 keV energy band) and the radio power at 1.4 GHz ($P_{1.4}$) for our sample of GRHs. The fit has been performed by using the form:

$$\log \left(\frac{P_{1.4 \text{ GHz}}}{3.16 \cdot 10^{24} h_{70}^{-1} \frac{\text{Watt}}{\text{Hz}}} \right) = A_f + b_f \log \left[\frac{L_X}{10^{45} h_{70}^{-1} \frac{\text{ergs}}{\text{s}}} \right] \quad (1)$$

where the best fit parameters are: $A_f = 0.159 \pm 0.060$ and $b_f = 1.97 \pm 0.25$.

Our findings are consistent with those of Enßlin and Röttgering (2002) who used 14 clusters with radio halos and found a correlation of the form $P_{1.4 \text{ GHz}} \propto L_X^{1.94}$. Using 16 clusters with GRHs Feretti (2003) found a correlation between the X-ray bolometric luminosity and the radio power at 1.4 GHz of the form $P_{1.4 \text{ GHz}} \propto (L_X^{\text{bol}})^{1.8 \pm 0.2}$. A consistent result is obtained with the data in Tab. 1 ($P_{1.4 \text{ GHz}} \propto (L_X^{\text{bol}})^{1.74 \pm 0.21}$).

Although the trend in Fig.1 appears quite stringent, one may wonder whether it could be affected by observational biases. It should be pointed out that most GRHs have been discovered by follow ups of radio halo candidates mostly identified from the NRAO VLA Sky Survey (NVSS, Condon et al. 1998).

In Fig.2 we plot the average radio surface brightness of GRHs at 1.4 GHz, normalized to the radio brightness of A3562 (open circle with the smallest X-ray luminosity),

Table 1. Radio and X-ray properties of cluster with GRHs (linear size $\sim 1 h_{70}^{-1}$ Mpc) in a Λ CDM cosmology. In Col.(1): Cluster name. Col.(2): Cluster redshift. Col.(3): Cluster temperature given in keV. Col.(4): X-ray luminosity in the energy range $[0.1 - 2.4]$ keV in unit of $h_{70}^{-2} 10^{44}$ erg/s. Col.(5): Bolometric X-ray luminosity in the energy range $[0.01 - 40]$ keV in unit of $h_{70}^{-2} 10^{44}$ erg/s. Col.(6): Radio power at 1.4 GHz in unit of $h_{70}^{-2} 10^{24}$ Watt/Hz. Col.(7): Large Linear Size (LLS) of the Radio Halo is in h_{70}^{-1} kpc. Ref. for the temperature data in brackets: (Z04) Zhang al. 2004 (XMM); (W00) White et al. 2000 (ASCA); (M96) Markevitch 1996 (ASCA); (m) mean value between Mushotzky & Scharf 1997 (ASCA) and Govoni et al. 2004 (Chandra); (e) Ebeling et al. 1996 (from L_x -T relation) ; (D93) David et al. 1993 (Einstein MPC+ Exosat + Ginga); (M98) Markevitch et al. 1998 (ASCA); (m1) mean value between Z04 and Pierre et al. 1999 (ASCA data); (H93) Hughes et al. 1993 (GINGA). Ref. for the X-ray luminosities in brackets: (B04) Boehringer et al 2004, (E98) Ebeling et al 1998, (E96) Ebeling et al 1996, (T96) Tsuru et al 1996, Ref. for the radio data in brackets: (L00) Liang et al. 2000 (ATCA) (F00) Feretti 2000, (B03) Bacchi et al 2003, (GF00) Giovannini & Feretti 2000, (V03) Venturi et al 2003, (GFG01) Govoni et al. 2001, (G05) Govoni et al. 2005, (FF03) Feretti et al. 2001, (m2) mean value between Kim et al. 1990 and Deiss et al. 1997

cluster's name	z	T [keV]	L_X [10^{44} erg/s]	L_{bol} [10^{44} erg/s]	$P_{1.4}$ [10^{24} Watt/Hz]	LLS [Mpc h_{70}^{-1}]
1E50657-558	0.2994	$13.59^{+0.71}_{-0.58}$ (Z04)	23.322 ± 1.84 (B04)	88.619 ± 7.00	28.21 ± 1.97 (L00)	1.43
A2163	0.2030	$13.29^{+0.64}_{-0.64}$ (W00)	23.435 ± 1.50 (B04)	82.021 ± 5.24	18.44 ± 0.24 (FF01)	1.86
A2744	0.3080	$8.65^{+0.43}_{-0.29}$ (Z04)	13.061 ± 2.44 (B04)	37.315 ± 6.97	17.16 ± 1.71 (GFG01)	1.64
A2219	0.2280	$9.52^{+0.55}_{-0.40}$ (W00)	12.732 ± 0.98 (E98)	40.293 ± 4.34	12.23 ± 0.59 (B03)	1.56
CL0016+16	0.5545	$9.13^{+0.24}_{-0.22}$ (W00)	18.829 ± 1.88 (T96)	51.626 ± 5.16	6.74 ± 0.67 (GF00)	0.79
A1914	0.1712	$10.53^{+0.51}_{-0.50}$ (W00)	10.710 ± 1.02 (E96)	33.738 ± 3.21	5.21 ± 0.24 (B03)	1.18
A665	0.1816	$8.40^{+1.0}_{-1.0}$ (M96)	9.836 ± 0.98 (E98)	25.130 ± 3.92	3.98 ± 0.39 (GF00)	1.69
A520	0.2010	$7.84^{+0.52}_{-0.52}$ (m)	8.830 ± 0.79 (E98)	22.841 ± 5.14	3.91 ± 0.39 (GFG01)	1.00
A2254	0.1780	$7.50^{+0.0}_{-0.0}$ (e)	4.319 ± 0.26 (E96)	11.076 ± 0.66	2.94 ± 0.29 (GFG01)	0.86
A2256	0.0581	$6.90^{+0.11}_{-0.11}$ (W00)	3.814 ± 0.16 (E96)	9.535 ± 0.42	0.24 ± 0.02 (F00)	0.85
A773	0.2170	$8.39^{+0.42}_{-0.42}$ (m)	8.097 ± 0.65 (E98)	21.728 ± 3.62	1.73 ± 0.17 (GFG01)	1.14
A545	0.1530	$5.50^{+6.20}_{-1.10}$ (D93)	5.732 ± 0.50 (B04)	12.608 ± 1.10	1.48 ± 0.06 (B03)	0.82
A2319	0.0559	$8.84^{+0.29}_{-0.24}$ (M98)	7.403 ± 0.41 (E96)	20.730 ± 1.14	1.12 ± 0.11 (F00)	1.01
A1300	0.3071	$9.42^{+0.26}_{-0.25}$ (m1)	14.114 ± 2.08 (B04)	33.870 ± 4.98	6.09 ± 0.61 (F00)	0.86
A1656	0.0231	$8.21^{+0.16}_{-0.16}$ (H93)	3.772 ± 0.10 (E96)	10.182 ± 0.26	$0.72^{+0.07}_{-0.04}$ (m2)	0.78
A2255	0.0808	$6.87^{+0.20}_{-0.20}$ (W00)	2.646 ± 0.12 (E96)	6.611 ± 0.30	0.89 ± 0.05 (G04)	0.88
A754	0.0535	$9.38^{+0.27}_{-0.27}$ (W00)	4.314 ± 0.33 (E96)	12.946 ± 0.98	1.08 ± 0.06 (B03)	0.96

Table 2. Parameters of the β -fit and cluster mass estimated for the 16 galaxy clusters with GRHs for which β -fits are available. Col.(1): Cluster name. Col.(2): β -parameter value with 1σ error. Col.(3): Core radius in units of h_{70}^{-1} kpc and corresponding uncertainty. Col.(4): Virial mass and is uncertainty in units of $h_{70}^{-1} 10^{15} M_{\odot}$. Col.(5): Virial radius in units of h_{70}^{-1} kpc. Col.(6): Mass estimated inside the core radius in units of $h_{70}^{-1} 10^{13} M_{\odot}$. Ref. for the (data) source in brackets: (a) Markevitch et. al 2002 (Chandra); (b) RB02 (ROSAT for β -fit and T as in table 1); (c) Govoni et al. 2001 (ROSAT); (d) Ettori & Fabian 1999 (ROSAT); (e) Ettori et. al 2004 (Chandra); (f) Feretti 2004 (Einstein); (g) Lemonon et al. 1997 (ROSAT).

cluster's name	β	r_c [kpc h_{70}^{-1}]	M_v [$10^{15} M_{\odot}$]	R_v [kpc h_{70}^{-1}]	M_c [$10^{13} M_{\odot}$]
1E50657-558(a)	0.70 ± 0.07	179 ± 18	3.43 ± 0.38	3301	9.50 ± 1.40
A2163 (b)	0.80 ± 0.03	371 ± 21	4.32 ± 0.26	3766	22.00 ± 1.84
A2744 (c)	1.00 ± 0.08	458 ± 46	2.87 ± 0.26	3096	22.10 ± 2.96
A2219 (d)	0.79 ± 0.08	343 ± 34	2.52 ± 0.28	3104	14.40 ± 2.16
CL0016+16 (e)	0.68 ± 0.01	237 ± 80	1.47 ± 0.05	2166	8.27 ± 0.38
A1914 (b)	0.75 ± 0.02	165 ± 80	2.90 ± 0.15	3356	7.28 ± 0.51
A665 (f)	0.74 ± 0.07	350 ± 35	1.97 ± 0.30	2933	12.10 ± 2.20
A520 (c)	0.87 ± 0.08	382 ± 50	2.22 ± 0.25	3018	14.50 ± 2.51
A2256 (b)	0.91 ± 0.05	419 ± 28	2.23 ± 0.13	3281	14.70 ± 1.28
A773 (c)	0.63 ± 0.07	160 ± 27	1.52 ± 0.19	2636	4.72 ± 0.98
A545 (d)	0.82 ± 0.08	286 ± 29	1.25 ± 0.84	2562	7.20 ± 4.89
A2319 (b)	0.59 ± 0.01	204 ± 10	1.71 ± 0.07	3009	5.95 ± 0.38
A1300 (g)	0.64 ± 0.01	171 ± 80	1.71 ± 0.06	2609	5.76 ± 0.33
A1656 (b)	0.65 ± 0.02	246 ± 15	1.83 ± 0.07	3136	7.38 ± 0.53
A2255 (b)	0.80 ± 0.05	419 ± 28	1.76 ± 0.12	2996	12.80 ± 1.22
A754 (b)	0.70 ± 0.03	171 ± 12	2.42 ± 0.11	3379	6.25 ± 0.52

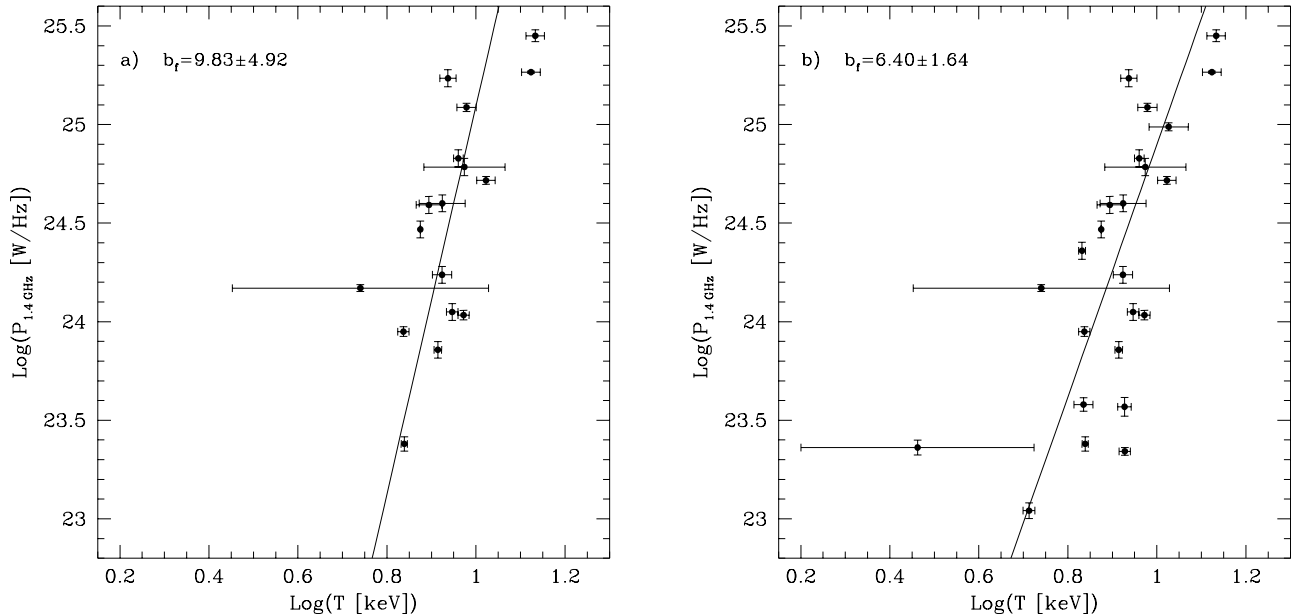


Figure 3. Panel a): correlation between the radio power at 1.4 GHz and the temperature for the GRHs; Panel b): correlation between the radio power at 1.4 GHz and the X-ray temperature for a total sample of 24 cluster with a GRHs or with a smaller size ($\sim 200 - 700$ kpc h_{50}^{-1}).

which is just visible in the NVSS, versus the X-ray luminosity of the hosting clusters. We note that all GRHs have a radio surface brightness which is well above that of A3562 (with the exception of A2256 not visible in the NVSS). The fact that clusters in the redshift range $z \sim 0.15 - 0.3$ have similar radio brightnesses indicates that the correlation in Fig.1 is not driven by the radio surface limit. Indeed, these clusters have $L_X \sim 3 \cdot 10^{44} - 3 \cdot 10^{45}$ erg/s and range over more than one order of magnitude in radio power, whereas the effect of brightness dimming, due to the small z -range, is limited to within a factor ~ 1.6 . We also note the presence of a trend, with the average radio brightness increasing with X-ray luminosity (see also Feretti 2004), which further supports the notion that the correlation in Fig.1 at high luminosities ($L_X \gtrsim 10^{45}$ erg/s) is not driven by selection effects. Furthermore, relatively deep upper limits for non radio-halo clusters are now available and in some cases lie well below (a factor of $\gtrsim 10$) the trend in Fig.1 at X-ray luminosities $\gtrsim 5 \cdot 10^{44}$ erg/s (Dolag 2006).

On the other hand one may argue that the NVSS tends to select only the most powerful GRHs associated with $L_X \lesssim 5 \cdot 10^{44}$ erg/s clusters. To evaluate the effect of a possible bias at these luminosities, we perform a fit by considering only GRH clusters with $L_X \gtrsim 5 \cdot 10^{44}$ and find a slope 2.22 ± 0.36 which is consistent within 1σ with Eq. 1.

Thus we conclude that despite the poor statistics, the derived correlations (Eq.1) stands on sound observational basis.

2.2 Radio Power–ICM temperature correlation

We also investigate the correlation between the radio power at 1.4 GHz and the X-ray ICM temperature. A $P_{1.4} - T$ correlation was first noted by Liang et al.(1999) and Co-

lafrancesco (1999); with a sample of only 8 radio halos the last author obtained a steep trend of the form $P_{1.4} \propto T^{6.25^{+6.25}_{-2.08}}$. In Fig. 3a we report the best fit for our sample. The fit has been performed using the form:

$$\log \left[\frac{P_{1.4 \text{ GHz}}}{3.16 \cdot 10^{24} h_{70}^{-1} \frac{\text{Watt}}{\text{Hz}}} \right] = A_f + b_f \log \left(\frac{T}{8 \text{ keV}} \right) \quad (2)$$

and best fit parameters are: $A_f = -0.390 \pm 0.139$ and $b_f = 9.83 \pm 4.92$. We note that the observed $P_{1.4} - T$ correlation is very steep, it seems rather a "wall" than a correlation and it is dominated by the large errors of the cluster temperatures available to date. In order to test the strength of this correlation we try to increase the sample by including also 7 additional clusters with smaller (size $\sim 200 - 700$ kpc h_{50}^{-1}) radio halos. In Fig. 3b we report the best-fit $P_{1.4} - T$ obtained for the extended sample, which has a slope $b_f = 6.40 \pm 1.64$. Given the large uncertainties we note that the two correlations are consistent at the 1σ level and, in addition, the value of the lower allowed bound of the two slopes is almost the same.

2.3 Radio Power – virial mass correlation

The most important correlation for our study is that between the virial mass (M_v) of a cluster and the radio power at 1.4 GHz. This correlation is indeed extensively used in the calculations of the RHLFs and number counts (Sec.7) and in constraining the values of the magnetic field in galaxy clusters to be used in our calculations (Sec.3). On the other hand, this is also the most difficult correlation to derive since it is very difficult to measure the cluster mass. Govoni et al. (2001) first obtained a correlation between the radio power and cluster gravitational mass (within $3 h_{50}^{-1}$

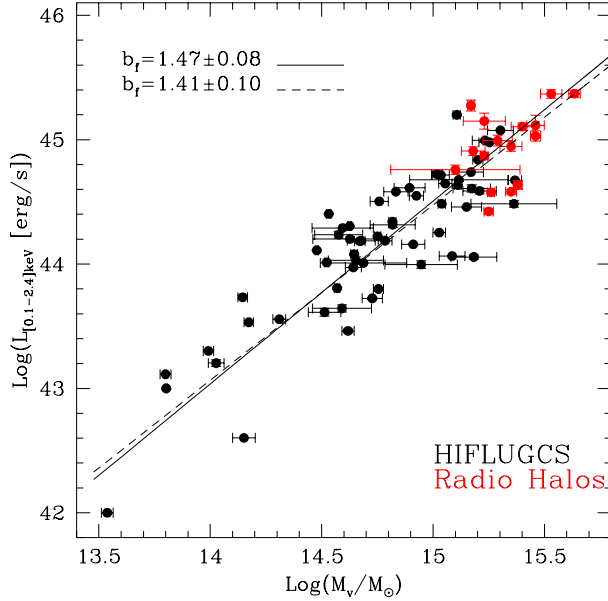


Figure 4. Correlation between the X-ray luminosity [0.1-2.4] keV and the virial cluster mass: for the HIFLUGCS sample (black points) plus the 16 clusters with GRHs (red points, excluding A2254 for which no information on the β -model are available) (solid line) and for the HIFLUGCS sample alone (dashed line).

Mpc radius) estimated from the surface brightness profile of the X-ray image using 6 radio halo clusters. This correlation was confirmed by Feretti (2003) who extended the sample to 10 cluster radio halos and obtained a best fit of the form $P_{1.4} \propto M^{2.3}$, where M is, again, the gravitational mass computed within $3 h_{50}^{-1}$ Mpc from the cluster center. However it should be pointed out that while the X-ray mass determination method gives good results in relaxed clusters, it may fail in the case of merging clusters (e.g., Evrard et al. 1996, Roettiger et al. 1996; Schindler 1996). This is because the merger may cause substantial deviation from hydrostatic equilibrium and spherical symmetry. As a result, the masses in merging clusters can be either overestimated (up to twice the true mass in the presence of shocks) or underestimated (since substructures tend to flatten the average density profile giving an underestimation of the order of 50 % of the true mass; see Schindler 2002). In addition, if the temperature systematically decreases with increasing radius, then the isothermal assumption leads to an overestimation of the cluster mass of about 30% at about six core radii (Markevitch et al. 1998).

The effect of the scattering produced by all these uncertainties can hopefully be reduced by making use of large cluster samples. Thus, we choose to obtain the $P_{1.4 GHz} - M_v$ correlation by combining the $L_x - M_v$ correlation, obtained for a large statistical sample of galaxy clusters, with the $P_{1.4} - L_x$ correlation previously derived (Eq.1, Fig. 1). We use a complete sample of the X-ray-brightest clusters (HIFLUGCS, the Highest X-ray FLUX Galaxy Cluster Sample) compiled by Reiprich & Böhringer (2002) (hereafter RB02). We use this sample of luminous clusters ($L_x \sim 10^{44} - 10^{45}$ erg s $^{-1}$) since it is large and homogeneously studied. It consists of 63 bright clusters with galactic latitude $|b_{l}| > 20^\circ$, flux

$f_X(0.1 - 2.4 \text{ keV}) \geq 2 \times 10^{-11}$ ergs s $^{-1}$ cm $^{-2}$ and it covers about 2/3 of the whole sky.

The clusters have been reanalyzed in detail by RB02 using mainly ROSAT PSPC pointed observations. RB02 report the value of β and core radius, r_c , for all the 63 clusters obtained by fitting the surface brightness profile of the X-ray image with a standard β -model. Then under the assumption that the intracluster gas is in hydrostatic equilibrium and isothermal (using the ideal gas equations), the gravitational cluster mass within a radius r is given by (e.g., Sarazin 1986):

$$M_{tot}(< r) = \frac{3K_B T r^3 \beta}{\mu m_p G} \left(\frac{1}{r^2 + r_c^2} \right), \quad (3)$$

Eq.3 gives the total (dark matter plus gas) mass of the cluster as a function of radius; then one must define a physically meaningful radius to compare masses of different clusters. It is frequently convenient to use r_{200} meaning the radius within which the mean total mass density is 200 times the critical density of the universe at the cluster redshift. This is because M_{200} , the mass contained within r_{200} , is usually taken as a good approximation of the virial mass since in the spherical collapse model the ratio between the average density within the virial radius and the mean cosmic density at redshift z is $\Delta_c = 18\pi^2 \simeq 178$ independent of the redshift for $\Omega_m = 1$ (e.g., Lacey & Cole 1993). In general, the value of Δ_c depends on the adopted cosmology. In the Λ CDM cosmology Δ_c is given by (Kitayama & Suto 1996):

$$\Delta_c(z) = 18\pi^2 (1 + 0.4093\omega(z)^{0.9052}), \quad (4)$$

where $\omega(z) \equiv \Omega_f(z)^{-1} - 1$ with:

$$\Omega_f(z) = \frac{\Omega_{m,0}(1+z)^3}{\Omega_{m,0}(1+z)^3 + \Omega_\Lambda}, \quad (5)$$

Thus, by using Eq.3 we calculate the virial radius, R_v , as the radius at which the ratio between the average density in the cluster and the mean cosmic density at the redshift of the cluster is given by $\Delta_c(z)$ (Eq.4). The virial mass, M_v , and the virial radius are thus related by:

$$R_v = \left[\frac{3M_v}{4\pi\Delta_c(z)\rho_m(z)} \right]^{1/3} \quad (6)$$

where $\rho_m(z) = 2.78 \times 10^{11} \Omega_{m,0} (1+z)^3 h^2 M_\odot \text{Mpc}^{-3}$ is the mean mass density of the universe at redshift z .

We estimate the virial mass in the Λ CDM cosmology for the 63 clusters of the HIFLUGCS sample using Eq. 3; the fit parameters (β and r_c corrected for a Λ CDM cosmology) and the temperature T are given in RB02. We have searched in the literature for β -fit parameters and T of the clusters with GRHs (ref. in Tab. 2) in order to estimate M_v also for these clusters. Since some clusters of the HIFLUGCS sample are also in our sample, we note that in the majority of these cases the fits to the mass profile (and T) given in RB02 leads to a virial mass which is consistent at 1σ level with the mass derived by making use of the parameters obtained from more recent observations in the literature (given in Tabs. 1, 2). The $L_x - M_v$ distribution of the combined sample is reported in Fig. 4. The presence of a relatively large dispersion indicates the difficulty in estimating the virial masses of the single objects and confirms the need of large samples in these studies. We note that the statistical distribution of clusters with GRHs is not different

from that of the HIFLUGCS sample. On the other hand, we note that clusters with known GRHs span a range in mass comparable to the mass-dispersion in the HIFLUGCS sample which is due to the different dynamical status of clusters in the sample and to the uncertainties in the measurements. This further strengthens the need of the approach followed in this Section, since a L_x (or $P_{1.4}$)– M_v fit based on GRHs alone would be affected by large uncertainties.

In order to better sample the region of higher X-ray luminosities and masses (typical of clusters with GRHs), we compute the L_x – M_v fit by combining the HIFLUGCS with the radio–halo sample. The fit has been performed using the form:

$$\log \left[\frac{L_x}{10^{44} h_{70}^{-1} \frac{\text{ergs}}{\text{s}}} \right] = A_f + b_f \log \left(\frac{M_v}{3.16 \times 10^{14} h_{70}^{-1} M_\odot} \right) \quad (7)$$

The best fit values of the parameters are: $A_f = -0.229 \pm 0.051$ and $b_f = 1.47 \pm 0.08$ ($b_f = 1.41 \pm 0.10$ is obtained with HIFLUGCS sample only).

In order to derive the $P_{1.4 \text{ GHz}} - M_v$ correlation for GRHs, we combine Eqs 7 and 1 and find :

$$\log \left[\frac{P_{1.4}}{3.16 \cdot 10^{24} h_{70}^{-1} \frac{\text{Watt}}{\text{Hz}}} \right] = (2.9 \pm 0.4) \log \left[\frac{M_v}{10^{15} h_{70}^{-1} M_\odot} \right] - (0.814 \pm 0.147) \quad (8)$$

Our $P_{1.4 \text{ GHz}} - M_v$ correlation is slightly steeper than that obtained with 10 clusters by Feretti (2003) ($P_{1.4 \text{ GHz}} \propto M^{2.3}$), which, however, was derived in an EdS cosmology by considering the mass within $3 h_{50}^{-1} \text{ Mpc}$ from the cluster centers, and not the virial mass.

3 EXPECTED CORRELATIONS AND MAGNETIC FIELD CONSTRAINTS

The main goal of this Section is to extract the values of the physical parameters to be used in the model calculations of Sec.4-6. The region of the physical parameters (in particular of B) is constrained by comparing the model expected and observed trends of the synchrotron power of GRHs with the mass (and temperature) of the parent clusters. As already discussed (Sec.2) it is unlikely that the observed correlations are driven by selection effects; however, it cannot be excluded that the detailed shape and scatter of these correlations might somewhat change with improved statistics, especially at low X-ray luminosities.

3.1 Radio power–cluster mass correlation

Cassano & Brunetti (2005) derived an expected trend between the bolometric radio power, P_R , and the virial cluster's mass and/or temperature. In the case of the GRHs, the mergers which mainly contribute to the injection of turbulence in the ICM are those with $r_s \geq R_H$, r_s being the stripping radius of the infalling sub-cluster (see Sec. 6 in CB05). It can be shown that, as a first approximation, the expected scaling $P_R - M_v$ is given by:

$$P_R \propto \frac{M_v^{2-\Gamma} B^2 n_e}{(B^2 + B_{cmb}^2)^2} \quad (9)$$

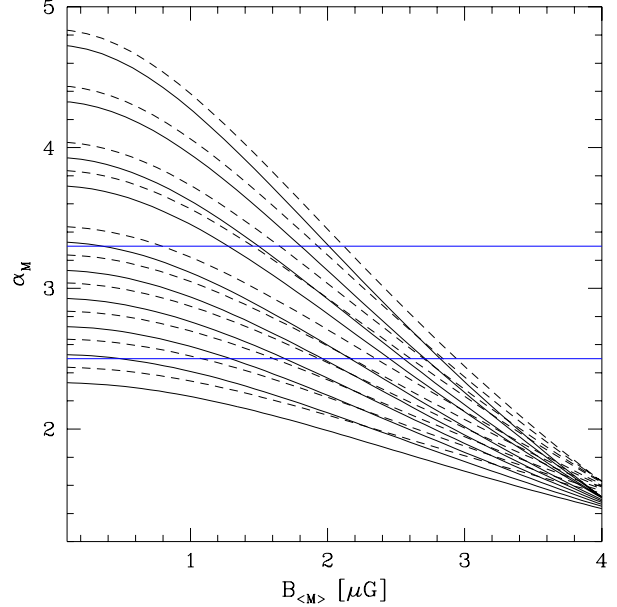


Figure 5. Expected slope of the $P_{1.4} - M_v$ correlation as a function of the magnetic field intensity in a cluster of mass $< M > = 1.6 \times 10^{15} M_\odot$. The calculations are obtained for $b=0.5, 0.6, 0.7, 0.8, 0.9, 1, 1.2, 1.3, 1.5$ and 1.7 (from bottom to top); $M_1 = 1.1 \times 10^{15} M_\odot$ and $M_2 = 2.5 \times 10^{15} M_\odot$ are adopted. The continuous lines are for $\Gamma \simeq 0.67$ and the dashed lines are for $\Gamma \simeq 0.56$. The two horizontal lines mark the 1σ value of the observed slope.

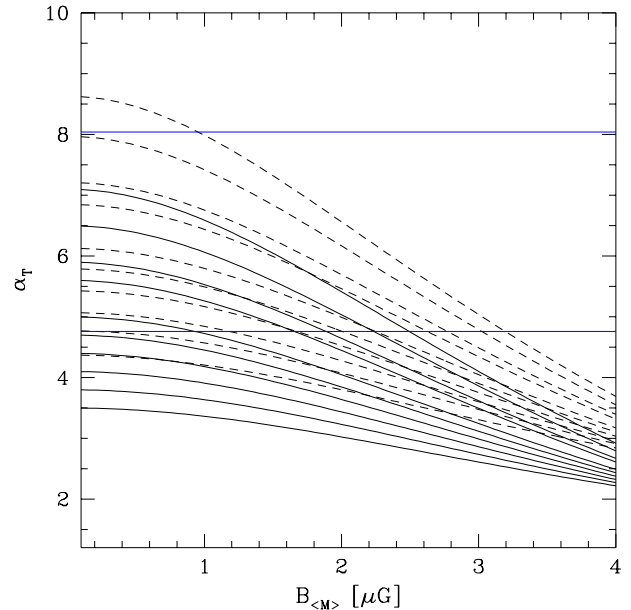


Figure 6. Expected slope of the $P_{1.4} - T$ correlation as a function of the magnetic field intensity in a cluster with temperature $< T > = 8 \text{ keV}$. The calculations are obtained for $b=0.5, 0.6, 0.7, 0.8, 0.9, 1, 1.2, 1.3, 1.5$ and 1.7 (from bottom to top); $T_1 = 6 \text{ keV}$ and $T_2 = 10 \text{ keV}$ are adopted. The continuous lines are for $\Gamma \simeq 0.67$ and the dashed lines are for $\Gamma \simeq 0.56$. The two horizontal lines mark the 1σ value of the observed slope.

where B is the rms magnetic field strength in the radio halo volume (particle pitch angle isotropization is assumed), $B_{cmb} = 3.2(1+z)^2 \mu G$ is the equivalent magnetic field strength of the CMB and n_e is the number density of relativistic electrons in the volume of the GRH. The parameter Γ is defined by $T \propto M^\Gamma$; we consider $\Gamma \simeq 2/3$ (virial scaling) and $\Gamma \simeq 0.56$ (e.g.; Nevalainen et al. 2000).

In this paper we release the assumption adopted in CB05 of a magnetic field independent of cluster mass and assume that the rms field in the emitting volume scales as $B = B_{<M>}(M / <M>)^b$, with $b > 0$ and $B_{<M>}$ the value of the rms magnetic field associated to a cluster with mass equal to the mean mass $<M>$ of the clusters sample. A scaling of the magnetic field intensity with the cluster mass is indeed found in numerical cosmological MHD simulations (e.g. Dolag et al. 2002, 2004). Dolag et al. (2002) found a scaling $B \propto T^2$ that would mean $B \propto M^{1.33}$ assuming the virial scaling or $B \propto M^{1.12}$ for $\Gamma \simeq 0.56$.

We assume that the number density of the relativistic electrons in galaxy clusters, n_e , does not depend on cluster mass. This is because there is no straightforward physical reason to believe that this value should scale systematically with M_v , and since only a relatively fast scaling of n_e with mass would significantly affect the radio power – mass trend (Eq. 9). It is indeed more likely that n_e may change from cluster to cluster, but that the major effect would simply be to drive some scattering on the $P_R - M_v$ trend (Eq. 9).

Given these assumptions Eq. 9 becomes:

$$P_R \propto \frac{M_v^{2-\Gamma} B_{<M>}^2 \cdot (M_v / <M>)^{2b}}{(B_{<M>}^2 \cdot (M_v / <M>)^{2b} + B_{cmb}^2)^2} \quad (10)$$

which has two asymptotic behaviors: $P_R \propto M_v^{2-\Gamma+2b}$ for $B_{<M>} \ll B_{cmb}$ and $P_R \propto M_v^{2-\Gamma-2b}$ for $B_{<M>} \gg B_{cmb}$. The observed correlations derived in Sect. 2 involve the monochromatic radio power at 1.4 GHz. How this monochromatic radio power can be scaled to P_R depends on the spectrum of radio halos. In the context of particle acceleration models (e.g., Brunetti et al. 2001, Ohno et al 2002, Kuo et al. 2003) the spectrum of radio halos is given by the superposition of spectra emitted from regions in the emitting volume with different magnetic field strenghts. It is expected to reach a peak at ν_b and then gradually drop as a power-law which should further steepen at higher frequencies. The break frequency can be expressed as a function of the cluster mass and of the rms field B in the emitting volume (CB05):

$$\nu_b \propto M^{2-\Gamma} \frac{B \eta_t^2}{(B^2 + B_{cmb}^2)^2} \quad (11)$$

If we adopt a power-law spectrum extending from the frequency of the peak to a few GHz, $P(\nu) \propto \nu^{-a}$, P_R and the monochromatic radio power at a fixed frequency ν_o ($\nu_o \geq \nu_b$) scale as $P(\nu_o)/P_R \propto (\frac{\nu_o}{\nu_b})^{a-1}$. This depends on the cluster mass (Eq.11):

$$\frac{P(\nu_o)}{P_R} \propto \frac{M_v^{(a-1)(2-\Gamma+b)}}{(B_{<M>}^2 (M_v / <M>)^{2b} + B_{cmb}^2)^{2(a-1)}} \quad (12)$$

thus in the case $B \ll B_{cmb}$ one has $P(\nu_o)/P_R \propto (\frac{M}{<M>})^{(a-1)(2-\Gamma+b)}$, while in the case $B \gg B_{cmb}$ one has $P(\nu_o)/P_R \propto (\frac{M}{<M>})^{(a-1)(2-\Gamma-3b)}$, which means that for $B \ll B_{cmb}$ the $P(\nu_o) - M$ trend is steeper than the $P_R - M$, while the opposite happens in the case $B \gg B_{cmb}$ (the two

Table 3. Values of α_M and η_t derived for relevant sets of b , $B_{<M>} [\mu G]$ parameters.

b	$B_{<M>} [\mu G]$	α_M	η_{min}	η_{max}
1.7	3.0	2.5	0.19	0.2
1.7	2.2	3.22	0.17	0.2
1.5	1.9	3.3	0.15	0.2
1.3	2.25	2.84	0.15	0.2
1.0	1.55	2.96	0.16	0.21
1.0	0.45	3.3	0.29	0.33
0.9	0.18	3.23	0.39	0.44
0.6	0.2	2.63	0.38	0.44

scaling should be equal for continuity for $B \sim B_{cmb}$). On the other hand, the trends of $P(\nu_o)/P_R$ with the cluster mass in massive galaxy clusters is rather weak because the observed radio spectral index between 327–1400 MHz is $a \sim 1.2$ (e.g., Feretti 2003) and because B in the most massive objects is probably close to B_{cmb} (Sec.3.3, Fig.7; Govoni & Feretti 2004). Thus, in order to compare the model expectations with the observations, we will safely assume the same scaling for monochromatic and total radio power.

In order to have a prompt comparison with observations we calculate the slope α_M of the $P_{1.4} - M$ correlation between two points as:

$$\alpha_M = \frac{\log(P_1/P_2)}{\log(M_1/M_2)} \quad (13)$$

Eq.13 can be compared with the observed slope to constrain the value of the magnetic field and of the slope, b , of the scaling between B and the cluster mass. The M_1 and M_2 values give the representative mass range spanned by the bulk of clusters with GRHs, while B_{cmb} should be calculated at the mean redshift of our sample ($<z> \simeq 0.19$). We point out that given $B_{<M>}$ and b , the values of B are fixed for all the values of the masses of the clusters in our sample.

In Fig.5 we report the expected slope α_M (Eq. 13) as a function of $B_{<M>}$. The different curves are obtained for different scaling-laws of the magnetic field with the cluster mass ($b = 0.5$ to 1.7 , see caption). Dashed lines refer to $\Gamma \simeq 0.56$ and solid lines to the virial case. The two blue horizontal lines (Fig.5) indicate the range of the observed slope ($\alpha_M = 2.9 \pm 0.4$).

Fig. 5 shows that there are values of $B_{<M>}$ and b for which the expected slope is consistent with the observed one. As a first result we find that with increasing b the values of $B_{<M>}$ should increase in order to match the observations (for example, $b \sim 0.6$ requires $B_{<M>} \sim 0.2 - 1.4 \mu G$ while $b \sim 1.7$ requires $B_{<M>} \sim 2 - 3 \mu G$). Finally, the asymptotic behavior of Eq.10, combined with the observed correlation (Eq. 8) allows to immediately constrain b : for $B_{<M>} \ll B_{cmb}$ one has $0.58(0.53) < b < 0.98(0.93)$ for the virial (non-virial) case, whereas in the case of $B_{<M>} \gg B_{cmb}$ the model expectations cannot be reconciled with the observations.

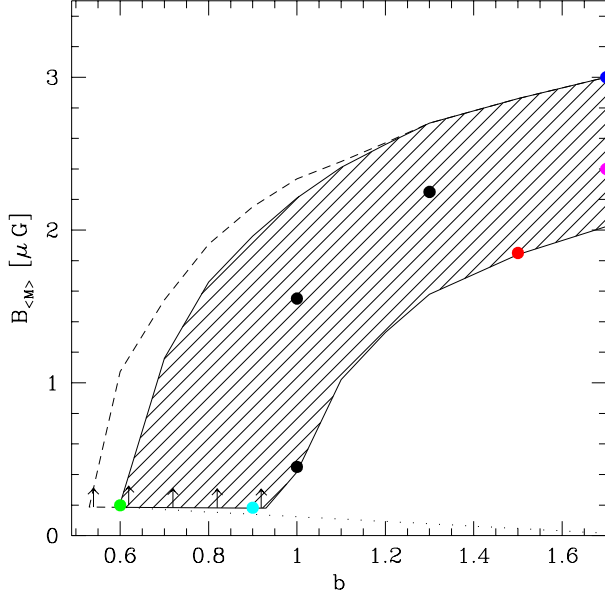


Figure 7. The region in the plane $(B_{<M>}, b)$ allowed from the observed $P_{1.4} - M_v$ and $P_{1.4} - T$ correlations is reported as a shadowed area; $\langle M \rangle = 1.6 \times 10^{15} M_\odot$. The dashed line indicate the upper bound of the allowed region obtained considering only the $P_{1.4} - M_v$ correlation. The coloured points indicate the relevant configurations of the parameters used in the statistical calculations in Sec.4-6 (Tab. 3). The vertical arrows indicate the IC limits on B .

3.2 Radio power–cluster temperature correlation

Since the temperature is related to the cluster mass, the radio power – mass correlation also implies a correlation between synchrotron radio power and cluster temperature. Thus, in order to maximize the observational constraints, an analysis similar to that of Sect. 3.1 can also be done for the radio power – temperature correlation ($P_R - T$). Combining Eq. 10 with the $M - T$ scaling law ($T \propto M^{2/3}$ for the virial case and $T \propto M^{0.56}$) one has:

$$P_R \propto \frac{T^{\frac{2}{\Gamma}-1} B_{<M>}^2 (T / \langle T \rangle)^{2b_T}}{(B_{<M>}^2 \cdot (T / \langle T \rangle)^{2b_T} + B_{cmb}^2)^2} \quad (14)$$

where $b_T = b/\Gamma$ with $\Gamma \simeq 2/3$ (virial case) or $\Gamma \simeq 0.56$ (non-virial case). The asymptotic behaviors of Eq. 14 are given by $P_R \propto T^{2/\Gamma-1+2b_T} (B_{<M>} \ll B_{cmb})$ and $P_R \propto M_v^{2\Gamma-1-2b_T} (B_{<M>} \gg B_{cmb})$.

As in Sec.3.1, here we can adopt the same scaling with T for both P_R and $P_{1.4}$ and compare the values of the expected slope with those of the observed one. We can calculate the slope α_T of the $P_{1.4} - T$ correlation between two points as:

$$\alpha_T = \frac{\log(P_1/P_2)}{\log(T_1/T_2)} \quad (15)$$

where T_1 and T_2 define the interval of temperature of our sample, $\langle T \rangle = 8$ keV is the mean temperature, and B_{cmb} is evaluated at $\langle z \rangle \simeq 0.19$. In Fig. 6 we report the slope α_T of the $P_{1.4} - T$ correlation as a function of the magnetic field strength in a average cluster, $B_{<M>}$. The different curves are obtained for different scaling-laws of the cluster magnetic fields with mass (i.e., temperature) ($b=0.5$ to 1.7). Dashed

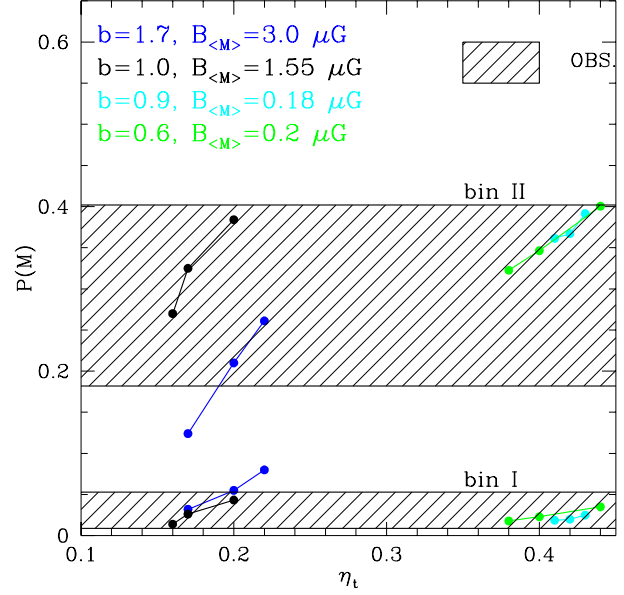


Figure 8. Probability to form GRHs at $0.05 \leq z \leq 0.15$ in the observed mass bin I: $0.95 - 1.9 \times 10^{15} M_\odot$ and at $0.05 \leq z \leq 0.2$ in bin II: $1.9 - 3.8 \times 10^{15} M_\odot$ as a function of η_t . The calculations are reported for the following representative cases: $b = 1.7$, $B_{<M>} = 3.0 \mu\text{G}$ (blue points); $b = 1.0$, $B_{<M>} = 1.55 \mu\text{G}$ (black points); $b = 0.9$, $B_{<M>} = 0.18 \mu\text{G}$ (cyan points) and $b = 0.6$, $B_{<M>} = 0.2 \mu\text{G}$ (green points). The bottom shadowed region marks the observed probability for GRHs in the mass bin I while the top shadowed region marks that in the mass bin II. The values of the observed probabilities are obtained by combining the results from Giovannini et al. 1999, Giovannini & Feretti 2000, and Feretti 2002. The observed probabilities for the bin I are calculated up to $z \leq 0.15$ to minimize the effect due to the incompleteness of the X-ray and radio catalogs used by these authors.

lines are for $\Gamma \simeq 0.65$ and continuous lines are for the virial case.

The horizontal blue lines mark the lower limit $\alpha_T \simeq 4.76$ and the upper limit $\alpha_T \simeq 8.05$ of the observed correlation. Fig. 6 shows that there is a range of values of the parameters $(B_{<M>}, b)$ for which the model is consistent with the observed slope. The relevant point is that, similarly to the case of the $P_{1.4} - M$ correlations, also in this case values of $B_{<M>} \gg B_{cmb}$ cannot be reconciled with observations: a clear upper boundary at $B < 3 \mu\text{G}$ is obtained for $B_{<M>}$.

3.3 Constraining the magnetic field

We combine the results obtained from the observed correlations (both $P_{1.4} - M_v$ and $P_{1.4} - T$) and the model expected trends to select the allowed region of the $(B_{<M>}, b)$ parameters. We consider the slope of the $P_{1.4} - T$ correlation $\alpha_T \simeq 6.4 \pm 1.64$ as derived for the extended sample of 24 galaxy clusters with giant and small radio halos. This is because what is important here is the allowed lower bound of the values of α_T which does not depend on the adopted sample (Sect. 2.2).

In Fig.7 we report the region of the plane $(B_{<M>}, b)$ allowed by the observed slopes at 1σ level. The lower bound of the $(B_{<M>}, b)$ region is due to the $P_{1.4} - M_v$ correlation while

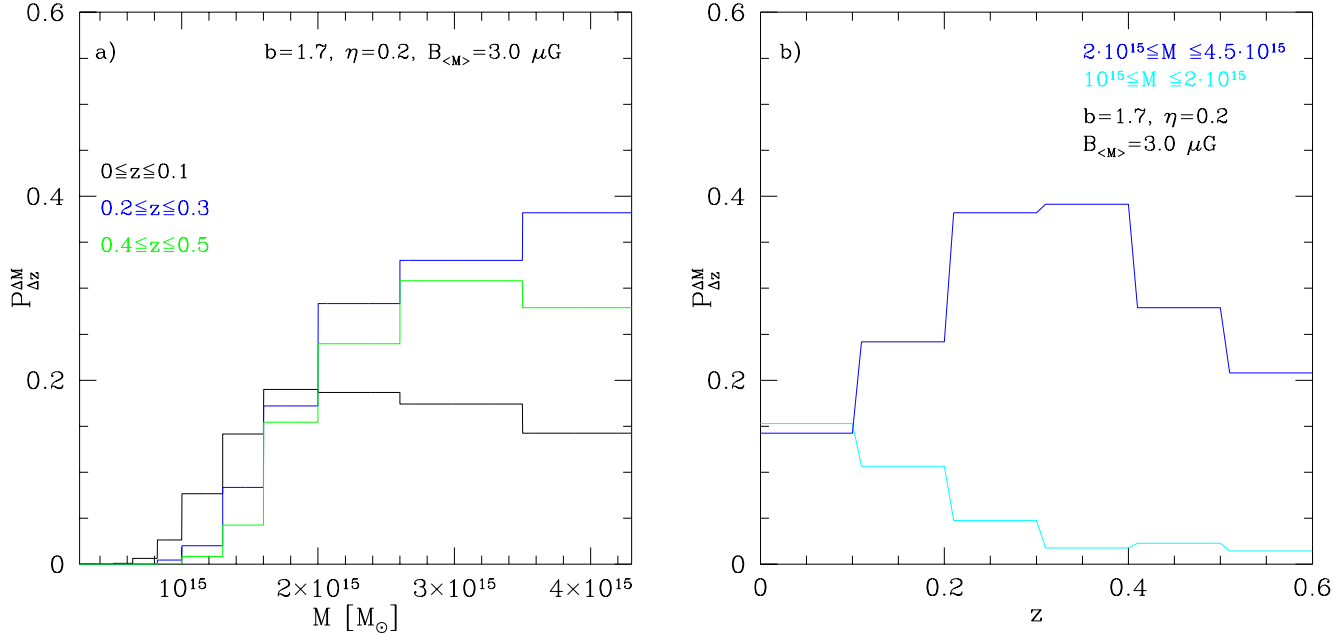


Figure 9. a) Occurrence of GRHs as a function of the cluster mass in three redshift bins: 0-0.1 (black line), 0.2-0.3 (blue line), 0.4-0.5 (green line). b) Occurrence of GRHs as a function of redshift in two mass bins: $[1-2] \times 10^{15} M_{\odot}$ (cyan line) and $[2-4.5] \times 10^{15} M_{\odot}$ (blue line). The calculation have been performed assuming: $b=1.7$, $B_{<M>} = 3.0 \mu\text{G}$, $\eta_t = 0.2$ in both panels.

the upper bound is mostly due to the $P_{1.4} - T$ correlation which is poorly constrained because of the very large statistical errors. This bound is however also limited by the $P_{1.4} - M_v$ correlation (Fig.7, dashed line).

An additional limit on $B_{<M>}$, also reported in Fig.7 (vertical arrows), can be obtained from inverse Compton (IC) arguments. Indeed a lower bound to the magnetic field strength can be inferred in order to not overproduce, via IC scattering of the photons of the CMB radiation, the hard-X ray excess fluxes observed up to now in a few clusters (e.g., Rephaeli & Gruber 2003, Fusco-Femiano et al 2003). In this case the value of the mean magnetic field intensity in the cluster volume can be estimated from the ratio between the hard-X ray and radio emission. The resulting value of the magnetic field should be considered as a lower limit because the IC emission may come from more external region with respect to the synchrotron emission (e.g., Brunetti et al. 2001, Kuo et al. 2003, Colafrancesco et al. 2005b) and also because, in principle, additional mechanisms may contribute to the hard-X ray fluxes (e.g., Fusco-Femiano et al. 2003). One of the best studied cases is that of the Coma cluster for which an average magnetic field intensity of the order of $B_{IC} \simeq 0.2 \mu\text{G}$ was derived (Fusco-Femiano et al. 2004). As a first approximation we can use this value to obtain the lower bound of B for each cluster mass from the scaling $B = B_{<M>}(M / \langle M \rangle)^b$.

The resulting $(B_{<M>}, b)$ region spans a wide range of values of B and b. An inspection of Fig.7 immediately identifies two allowed regimes: a super-linear scaling ($b > 1$) with relatively high values of B and a sub-linear scaling ($b < 1$) with lower values of B.

All the calculations we will report in the following sections are carried out by assuming representative values of

$(B_{<M>}, b)$ inside the constrained region (Fig. 7 coloured filled dots and Tab.3).

4 PROBABILITY TO FORM GIANT RADIO HALOS

4.1 Probability of radio halos and constraining η_t

In this Section we derive the probability with cluster mass to find GRHs in the redshift range $z=0-0.2$. The byproduct of the Section is to calibrate the model by requiring that the expected fraction of cluster with GRHs is consistent with the observational constraints. This allows to select a range of values of the parameter η_t , which is the ratio between the energy injected in the form of magnetosonic waves and the PdV work done by the infalling subclusters in passing through the most massive one. η_t is a free parameter in our calculations since the fraction of the energy which goes into the form of compressible modes is likely to depend on the details of the driving force.

In the conservative case of solenoidal forcing (and beta of plasma $\gg 1$) this fraction is expected to scale with $\mathcal{M}_s^2 \mathcal{R}_e$ (with $\mathcal{M}_s < 1$, the turbulent Mach number) for $\mathcal{M}_s^2 \mathcal{R}_e < 10$ and with a flatter slope for larger values (Bertoglio et al. 2001). Assuming a Reynolds number (at the injection scale, i.e., hundreds of Kpc) in hot and magnetized galaxy clusters $\mathcal{R}_e \gtrsim 10^3$ (see discussion in Lazarian 2006; Brunetti 2006) and a turbulent energy of the order of $\sim 20\%$ of the thermal energy (CB05), from Fig. 8 in Bertoglio et al. (2001) one finds a reference value $\eta_t \sim 0.1$ which may be even larger in the case of compressible driving.

Radio halos are identified with those objects in a synthetic cluster population with a synchrotron break frequency (Eq.11) $\nu_b \gtrsim 200 \text{ MHz}$ in a region of $1 \text{ Mpc } h_{50}^{-1}$ size. In

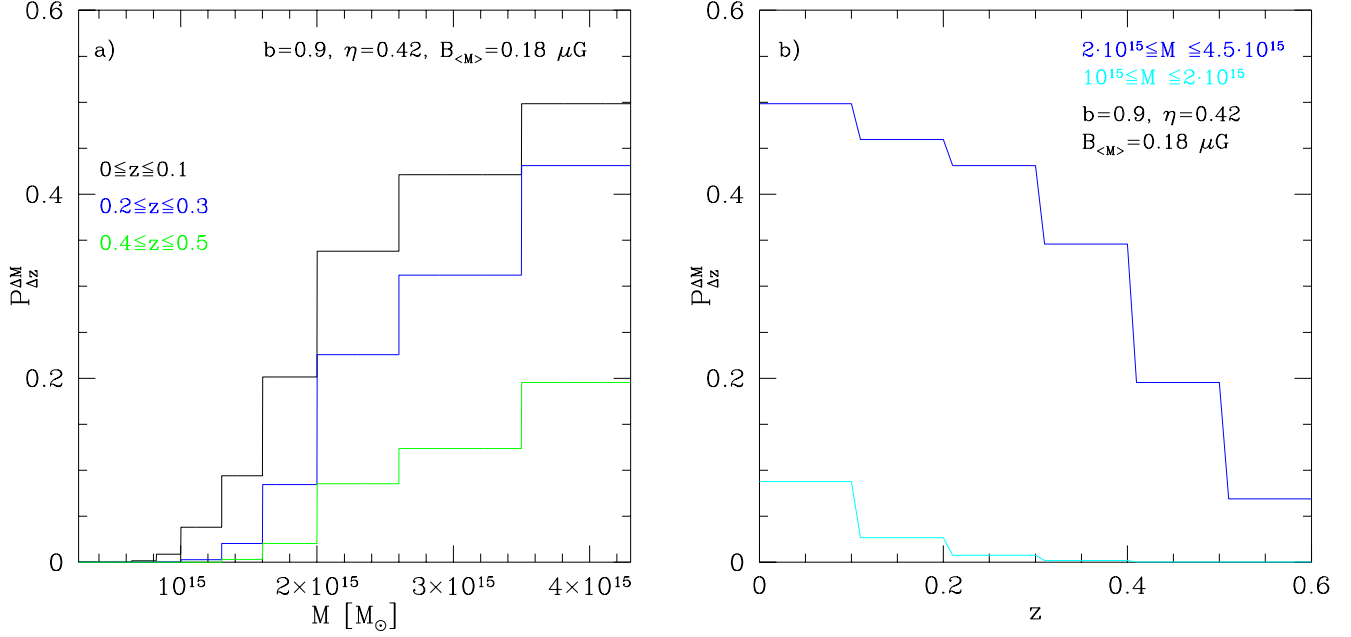


Figure 10. a) Occurrence of GRHs as a function of the cluster mass in three redshift bins: 0-0.1 (black line), 0.2-0.3 (blue line), 0.4-0.5 (green line). b) Occurrence of GRHs as a function of redshift in two mass bins: $[1-2] \times 10^{15} M_{\odot}$ (cyan line) and $[2-4.5] \times 10^{15} M_{\odot}$ (blue line). The calculation have been performed assuming: $b=0.9$, $B_{<M>} = 0.2 \mu G$, $\eta_t = 0.42$ in both panels.

CB05 it was assumed that the magnetic field in the radio halo volume is independent from the cluster mass and it is $B \simeq 0.5 \mu G$. Then $\nu_b \propto M^{2-\Gamma}$ and consequently massive clusters are expected to be favourite in forming GRHs. CB05 indeed showed that the expected fraction of clusters with GRHs naturally shows an abrupt increase with cluster mass, and that the observed fractions (20-30 % for $M > 2 \times 10^{15} M_{\odot}$ clusters, 2-5 % for $M \sim 10^{15} M_{\odot}$ clusters and negligible for less massive objects) can be well reconciled with the model expectations by assuming $\eta_t \sim 0.24 - 0.34$.

In the present paper we assume that the rms magnetic field depends on the cluster mass and this should affect the synchrotron break frequency (Eq. 11) and the occurrence of GRHs with cluster mass. On the other hand, in Sect. 3.3 we have also shown that the comparison between the expected and observed trends between radio power and cluster mass (and temperature) helps in constraining the range of values which can be assigned to the magnetic field in clusters.

Thus our calculations of the occurrence of GRHs ($z \leq 0.2$) and the selection of the values of η_t necessary to reproduce the observations should be performed within the dashed region in Fig.7.

To calculate the expected probabilities to form radio halos we first run a large number, \mathcal{N} , of trees for different cluster masses at $z = 0$, ranging from $\sim 5 \times 10^{14} M_{\odot}$ to $\sim 6 \times 10^{15} M_{\odot}$. Then we choose different mass bins ΔM and redshift bins Δz in which to perform our calculations. Thus, for each mass M , we estimate the formation probability of GRHs in the mass bin ΔM and in the redshift bin Δz as (CB05):

$$f_M^{\Delta M, \Delta z} = \frac{\sum_{j=1}^{\mathcal{N}} t_u^j}{\sum_{j=1}^{\mathcal{N}} (t_u^j + t_d^j)} \quad (16)$$

where t_u is the time in the redshift interval Δz that the cluster spends in the mass bin ΔM with $\nu_b \geq 200$ MHz and t_d is the time that the same cluster spends in ΔM with $\nu_b < 200$ MHz. The total probability of formation of GRHs in the mass bin ΔM and in the redshift bin Δz is obtained by combining all the contributions (Eq. 16) weighted with the present day mass function of clusters given by the Press & Schechter mass function.

To have a prompt comparison with present observational constraints, we calculate the probability to form GRHs at $z \lesssim 0.2$ in the two observed mass bins: bin I ($[0.95 - 1.9] \times 10^{15} M_{\odot}$) and bin II ($[1.9 - 3.8] \times 10^{15} M_{\odot}$).

As an example, in Fig. 8 we report these probabilities in both bin I and bin II as a function of η_t for three representative cases which nicely sample the region in Fig.7: $b = 1.7$, $B_{<M>} = 3.0 \mu G$ (blue points); $b = 1.0$, $B_{<M>} = 1.55 \mu G$ (black points); $b = 0.9$, $B_{<M>} = 0.18 \mu G$ (cyan points); $b = 0.6$, $B_{<M>} = 0.2 \mu G$ (green points).

The bottom shadowed region in Fig. 8 marks the observed probability for GRHs in the mass bin I while the top shadowed region marks that in the mass bin II. Fig. 8 shows that it is possible to find a range of values of the parameter η_t for which the theoretical expectations are consistent with the observed statistics in both the mass bins. However we note that the requirement in terms of energy of the MS modes increases with decreasing the magnetic field: it goes from $\eta_t \sim 0.15 - 0.2$ for intermediate-large values of B up to $\eta_t \sim 0.5$ at the lower bound of the allowed B strengths.

The fact that the magnetic field depends on the cluster mass is reflected in the different behavior that the various selected configurations of parameters may have in Fig. 8 in the two mass bins: one configuration of parameters may be favoured in a mass bin with respect to another configuration but disfavoured in the other mass bin. This is related to the

transition from IC dominance ($B < B_{cmb}$) to synchrotron dominance ($B > B_{cmb}$) that occurs in going from the bin I to the more massive clusters of bin II. In the case of IC dominance an increase of B does not significantly affect the particle energy losses, it causes an increase of ν_b (Eq.11) and thus an increase of the probability to have GRHs. On the other hand, in the case of synchrotron dominance the particle energy losses increase and consequently ν_b decreases (Eq.11) as well as the probability to form GRHs.

For this reason, given η_t , the ratio between the probability to form GRHs in the bin I and in the bin II is expected to decrease with increasing b , as larger values of b yield a more rapid increase of B with cluster mass (Fig.8).

In Tab.3 we report the maximum and the minimum values of η_t ($\eta_{t,max}$ and $\eta_{t,min}$) for which the model reproduces the observed probabilities (1 σ limits) in both the mass bins. The results are given for the relevant ($B_{<M>}, b$) configurations reported in Fig. 7. In agreement with the above discussions, one might notice that in the case of IC dominance a larger magnetic field implies a smaller energetic request (smaller $\eta_{t,max}$).

4.2 Probability of radio halos with M_v and evolution with z

In this Section we calculate the expected probability to form GRHs with cluster mass without restricting ourselves to the mass bins considered by present observations (bin I and bin II in Fig. 8) and calculate the evolution of this probability with redshift. In doing these calculations we use the values of η_t as constrained in Tab.3 within the region ($B_{<M>}, b$) of Fig.7, and make the viable (and necessary) assumption that the value of η_t (i.e., efficiency of turbulence in going into MS modes) is constant with redshift.

A detailed calculation of the acceleration efficiency and of the probability to have GRHs requires detailed Monte-carlo calculations (see Sec. 6 of CB05) essentially because at each redshift the acceleration is driven by MS modes injected in the ICM from the mergers that the cluster experienced in the last few Gyr at that redshift. However, to readily understand the model results reported in the following, we may use the simplified formula Eq. (11) which describes the approximate trend of the break frequency with cluster mass. The scaling $B \propto M^b$ adopted in this paper implies that the synchrotron losses overcome the IC losses first in the more massive objects. Clusters of smaller mass in our synthetic populations have $B \ll B_{cmb}$ and this implies (Eq.11) $\nu_b \propto M^{2-\Gamma+b} (1+z)^{-8}$ so that the probability to form GRHs in these clusters increases with the cluster mass ($2 - \Gamma + b > 0$ always) and decreases with redshift. In the case of more massive clusters the situation may be more complicated. Indeed for these clusters there is a value of the mass, M_* , for which the cluster magnetic field becomes equal to B_{cmb} . For $M > M_*(z)$ it is $\nu_b \propto M^{2-\Gamma-3b}$ (Eq. 11) and thus the probability to form GRHs would decrease as the mass becomes larger (given the lower bound of the slope b as constrained in Fig. 7, it is $2 - \Gamma - 3b < 0$). In these cases, at variance with the smaller clusters, the occurrence of GRHs with z is only driven by the cosmological evolution of the cluster-merger history (which drives the injection of turbulence) rather than by the dependence of the IC losses with z (at least up to a redshift for which $B \sim B_{cmb}(z)$). As

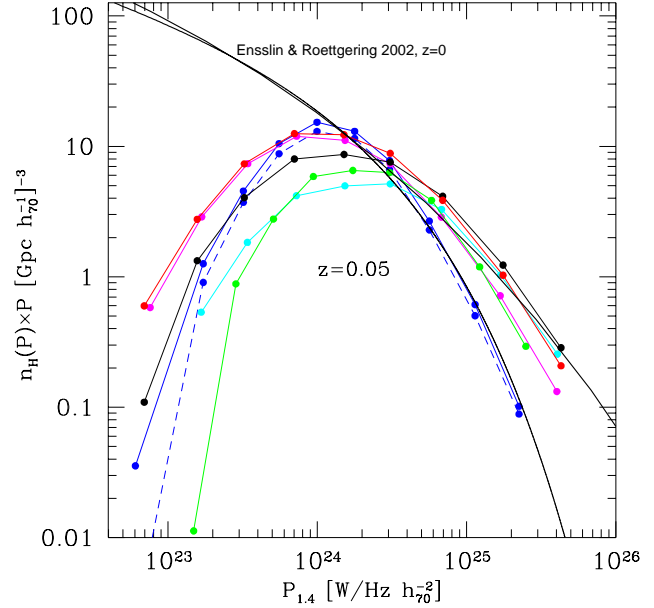


Figure 11. Expected RHLFs at $z \simeq 0.05$ (coloured lines with dots) obtained assuming: $b=1.7$, $B_{<M>} = 3.0\mu\text{G}$ (blue lines: $\eta_t = 0.2$ (solid line) and $\eta_t = 0.19$ (dashed line)); $b=1.7$, $B_{<M>} = 2.2\mu\text{G}$ and $\eta_t = 0.2$ (magenta line); $b=1.5$, $B_{<M>} = 1.9\mu\text{G}$ and $\eta_t = 0.2$ (red line); $b=0.9$, $B_{<M>} = 0.18\mu\text{G}$ and $\eta_t = 0.39$ (cyan line); $b=0.6$, $B_{<M>} = 0.2\mu\text{G}$ and $\eta_t = 0.38$ (green line); $b=1.0$, $B_{<M>} = 0.45\mu\text{G}$ and $\eta_t = 0.33$ (black line). For a comparison we report the range of Local RHLF obtained by E&R02 (black solid thick lines).

a consequence, the general picture is that going from smaller to larger masses, the probability should reach a max value around M_* for which $B \sim B_{cmb}(z)$, and then it should start to smoothly decrease. The value of this mass increases with z and depends on the scaling law of B with M . It is:

$$M_*(z) \simeq \langle M \rangle \left(\frac{3.2(1+z)^2}{B_{<M>}(\mu\text{G})} \right)^{1/b} \quad (17)$$

In order to show in some detail this complex behavior in the following we analyze two relevant examples.

4.2.1 An example with super-linear scaling: large B

As a first example we focus on the case of a super-linear scaling. In Fig. 9, we report the occurrence of GRHs as a function of the cluster mass in three redshift bins (panel a)) and the occurrence of GRHs as a function of redshift in two mass bins (panel b)). These calculations have been performed using $b = 1.7$ and $B_{<M>} = 3\mu\text{G}$ which are allowed from the observed correlations. We adopt $\eta_t = 0.2$ which is in the corresponding range of values obtained in Sec. 5 (see Tab. 3) in order to reproduce the observed probability of GRHs at $z < 0.2$. One finds that at lower redshifts ($z \lesssim 0.1$) the probability to form GRHs increases with the mass of the clusters up to $M_* \sim 2 \times 10^{15} M_\odot$, while for $M \gtrsim M_*$ synchrotron losses become dominant and this causes the decrease of the probability for $M \gtrsim M_*$. The mass at which $B \sim B_{cmb}(z)$ increases as $(1+z)^{2/b}$ and this causes the

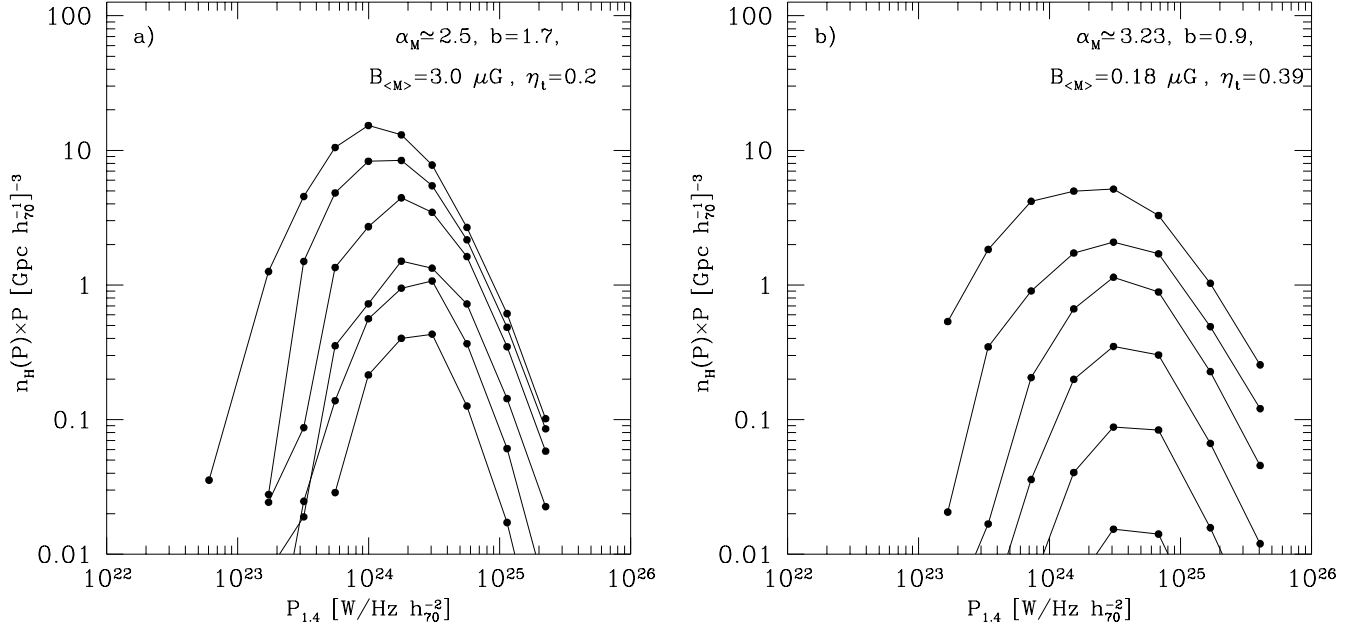


Figure 12. Evolution of RHLFs with redshift. The RHLFs are reported from redshifts 0-0.1 to 0.5-0.6 (curves from top to bottom). Calculations are developed for: Panel a) $b=1.7$, $B_{<M>} = 3.0 \mu\text{G}$, $\eta_t = 0.2$, $\alpha_M \simeq 2.5$ and Panel b) $b=0.9$, $B_{<M>} = 0.18 \mu\text{G}$, $\eta_t = 0.39$, $\alpha_M \simeq 3.23$.

shift with z of the value of the cluster mass at which the maximum of the probability is reached.

Fig.9b shows the occurrence of GRHs with z . In the higher mass bin ($2 \cdot 10^{15} \leq M \leq 4.5 \cdot 10^{15}$) the occurrence increases up to $z \sim 0.4$ and then start to drop. In this very massive clusters the magnetic field is larger than $B_{cmb}(z)$ at any redshift and thus the synchrotron losses are always the dominant loss term. The behavior of the probability with z in this case is essentially due to the fact that the bulk of turbulence in these massive clusters is injected preferentially between $z \sim 0.2-0.5$. A different behavior is observed in the lower mass bin ($10^{15} \leq M \leq 2 \cdot 10^{15}$) where the occurrence of GRHs decreases with redshift. This is because clusters with these lower masses have always $B < B_{cmb}(z)$.

4.2.2 An example with sub-linear scaling: small B

As a second example we focus on a sublinear scaling b . In Fig. 10 we report the occurrence of GRHs as a function of the cluster mass in three redshift bins (panel a)) and the occurrence of GRHs as a function of redshift in two mass bins (panel b)). The calculations have been performed using $b = 0.9$ and $B_{<M>} = 0.2 \mu\text{G}$, which are allowed from the correlations, and adopting a corresponding $\eta_t = 0.42$, which is within the range of values obtained in Sec. 5 (see Tab. 3) in order to reproduce the observed probability of formation of GRHs at redshift $z < 0.2$. In this case at any redshift the probability to form GRHs increases with the mass of the clusters. Indeed the magnetic field in these clusters is always $B \ll B_{cmb}(z)$ (for all redshifts and masses) and the IC losses are always the dominant loss term. In addition, as expected, in both the considered mass bins the probability to form GRHs decreases as a function of redshift, due to the increase of the IC losses (Fig. 10, panel b)).

5 LUMINOSITY FUNCTIONS OF GIANT RADIO HALOS

In this Section we derive the expected luminosity functions of giant radio halos (RHLFs). Calculations for the RHLFs are carried out within the $(B_{<M>}, b)$ region of Fig. 7 by adopting the corresponding values of η_t which allow to match the GRH occurrence at $z < 0.2$. First we use the probability $P_{\Delta z}^{\Delta M}$ to form GRHs with the cluster's mass to estimate the mass functions of GRHs ($dN_H(z)/dM dV$):

$$\frac{dN_H(z)}{dM dV} = \frac{dN_{cl}(z)}{dM dV} \times P_{\Delta z}^{\Delta M} = n_{PS} \times P_{\Delta z}^{\Delta M}, \quad (18)$$

where $n_{PS} = n_{PS}(M, z)$ is the Press & Schechter (1974) mass function whose normalization depends essentially by σ_8 (present-day rms density fluctuation on a scale of $8h^{-1}$ Mpc) and Ω_o ; we use $\sigma_8 = 0.9$ in a $\Omega_o = 0.3$ universe. We stress that we use n_{PS} since our model is based on the Press & Schechter formalism.

The RHLF is thus given by:

$$\frac{dN_H(z)}{dV dP_{1.4}} = \frac{dN_H(z)}{dM dV} \frac{dP_{1.4}}{dM}. \quad (19)$$

$dP_{1.4}/dM$ depends on the adopted $(B_{<M>}, b)$ since each allowed configuration in Fig. 7 selects a value of the slope of $P_{1.4} - M_v$ (e.g., Tab. 3) which is consistent (at 1σ) with the value of the observed slope obtained with present observations ($\alpha_M = 2.9 \pm 0.4$; see Sec. 3). In particular from Fig. 5 one has that, for a given b , larger values of the magnetic field select smaller values of the slope of the $P_{1.4} - M_v$ correlation (and viceversa).

In Fig.11 we report the Local RHLFs (number of GRHs per comoving Gpc^3 as a function of the radio power) as expected from our calculations. The most interesting feature in the RHLFs is the presence of a cut-off/flattening at low

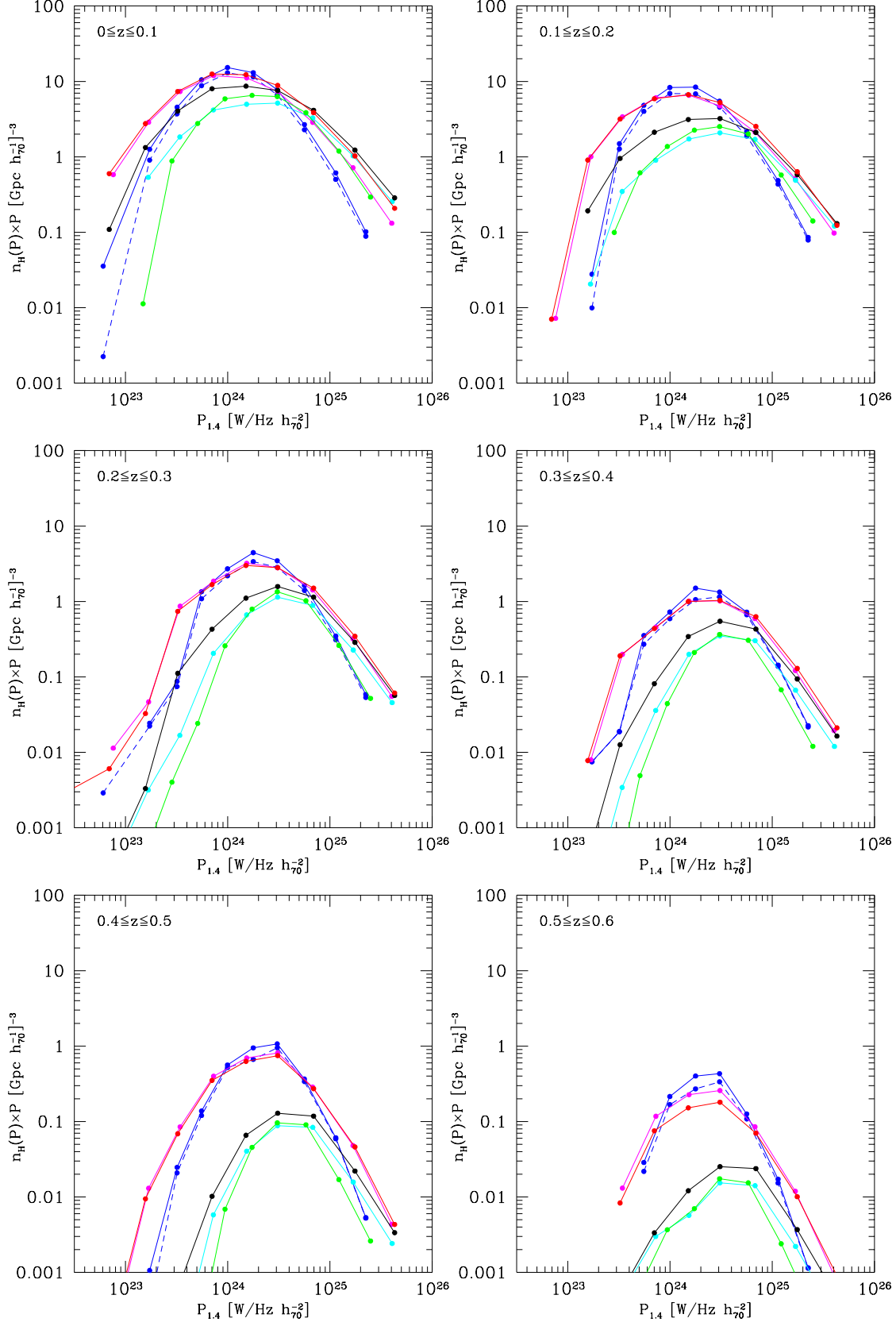


Figure 13. Expected RHLFs in 6 redshift bins (as reported in the panels). Calculations are performed by using the following values of the parameters : $b=1.7$, $B_{<M>} = 3.0\mu\text{G}$ (blue lines: $\eta_t = 0.2$ (solid lines) and $\eta_t = 0.19$ (dashed lines)); $b=1.7$, $B_{<M>} = 2.2\mu\text{G}$ and $\eta_t = 0.2$ (magenta lines); $b=1.5$, $B_{<M>} = 1.9\mu\text{G}$ and $\eta_t = 0.2$ (red lines); $b=0.9$, $B_{<M>} = 0.18\mu\text{G}$ and $\eta_t = 0.39$ (cyan lines); $b=0.6$, $B_{<M>} = 0.2\mu\text{G}$ and $\eta_t = 0.38$ (yellow lines); $b=1.0$, $B_{<M>} = 0.45\mu\text{G}$ and $\eta_t = 0.33$ (black lines).

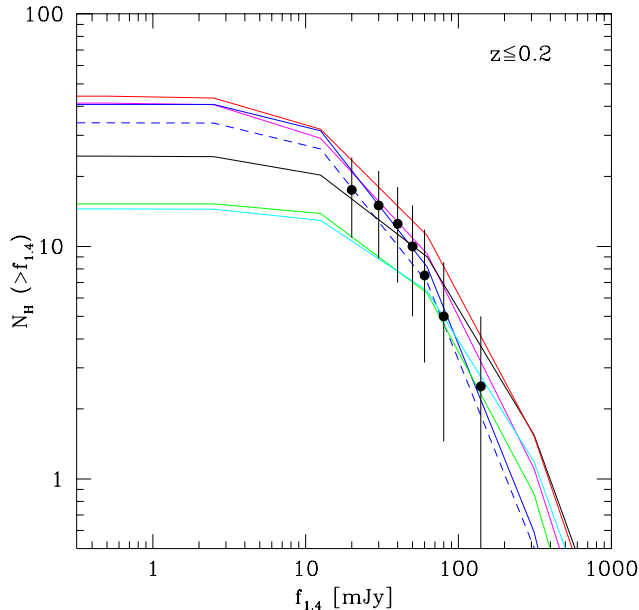


Figure 14. Number of expected GRHs above a given radio flux at 1.4 GHz from a full sky coverage up to $z \leq 0.2$ (the colour code is that of Fig. 11). The black points are the data taken from Giovannini et al. (1999) and corrected for the incompleteness of their sky-coverage ($\sim 2\pi$ sr).

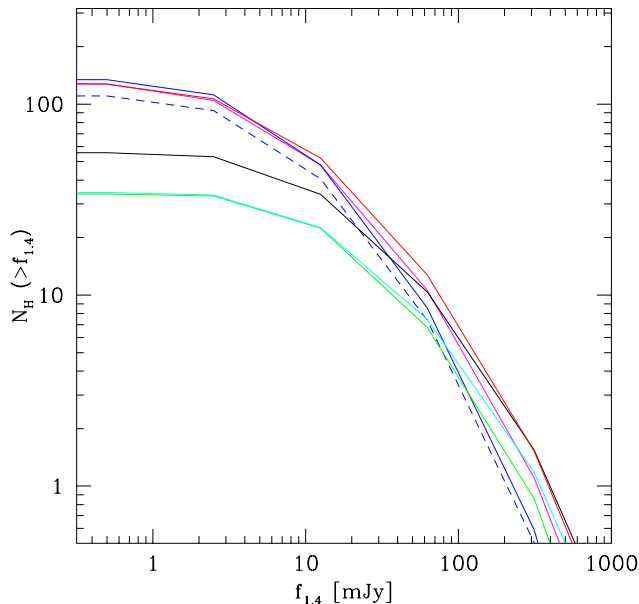


Figure 15. Number of expected GRHs from the whole universe above a given radio flux at 1.4 GHz. The colour code is the same of Fig. 11.

radio powers. This flattening is a unique feature of particle acceleration models since it marks the effect of the decrease of the efficiency of the particles acceleration (in 1 Mpc h_{50}^{-1} cube) in the case of the less massive galaxy clusters. We stress that this result does not depend on the particular choice of the parameters.

To highlight the result, in Fig. 11 we also compare our RHLFs with the range of Local ($RHLFs$)_{E&R} (black solid lines) reported by Enßlin & Röttgering (2002). These ($RHLFs$)_{E&R} are obtained by combining the X-ray luminosity function of clusters with the radio-X-ray correlation for GRHs and assuming that a constant fraction, $f_{rh} = 1/3$, of galaxy clusters have GRHs independently from the cluster mass (see Enßlin & Röttgering 2002).

The most important difference between the two expectations is indeed that a low-radio power cut-off does not show up in the ($RHLFs$)_{E&R} in which indeed the bulk of GRHs is expected at very low radio powers. The agreement between the two Local RHLFs at higher synchrotron powers is essentially because the derived occurrence of GRHs in massive objects (Sect. 4.2) is in line with the fraction, $f_{rh} = 1/3$, adopted by Enßlin & Röttgering (2002).

In Fig. 12 we report the RHLFs expected by our calculations in different redshift bins. The calculations are performed by using two relevant sets of parameters (a super-linear and a sub-linear case as given in the caption of Fig. 12) allowed from the observed correlations. With increasing redshift the RHLFs decrease due to the evolution of the clusters mass function with z and to the evolution of the probability to form GRHs with z .

Fig. 12, allows to readily appreciate the different behavior of the RHLFs in the case of a super-linear scaling of B with M , $b = 1.7$, (Fig. 12, Panel a)) and of a sub-linear scaling, $b = 0.9$ (Fig. 12, Panel b)): the evolution with redshift in the Panel b) (sub-linear case) is faster than that in the Panel a) (super-linear case). This difference is driven by the probability to form GRHs as a function of redshift in the two cases: in the super-linear case the probability to form GRHs does not decrease rapidly with z , while a rapid decrease of such a probability is obtained in the sub-linear case (see also Figs. 9, 10 Sect. 6).

In Fig. 13 we report the RHLFs obtained by our calculations by adopting the selected set of configurations given in Tab. 3 (colour code is the same of Fig. 7). The combination of these configurations define a bundle of expected RHLFs which determines the range of the possible RHLFs. All the calculations are performed for the corresponding range of values of η_t which allow to be consistent with the observed probability to form radio halos at $z \lesssim 0.2$. One finds that with increasing redshift the bundle of the RHLFs broadens along the $n_H(P) \times P$ axis. This is again due to the different evolutions of the probability to form GRHs with z of the super-linear and sub-linear cases.

6 NUMBER COUNTS OF GIANT RADIO HALOS

In this Section we derive the expected number counts of giant radio halos (RHNCs). This will allow us to perform a first comparison between the model expectations and the counts of GRHs which can be derived from present observations, but also to derive expectations for future observations. As for the case of the RHLFs, in calculating the RHNCs we adopt the configurations of parameters which allow to reproduce the observed probabilities of GRHs at $z < 0.2$. However, we point out that the fact that our expectations are consistent with the observed probability to form GRHs

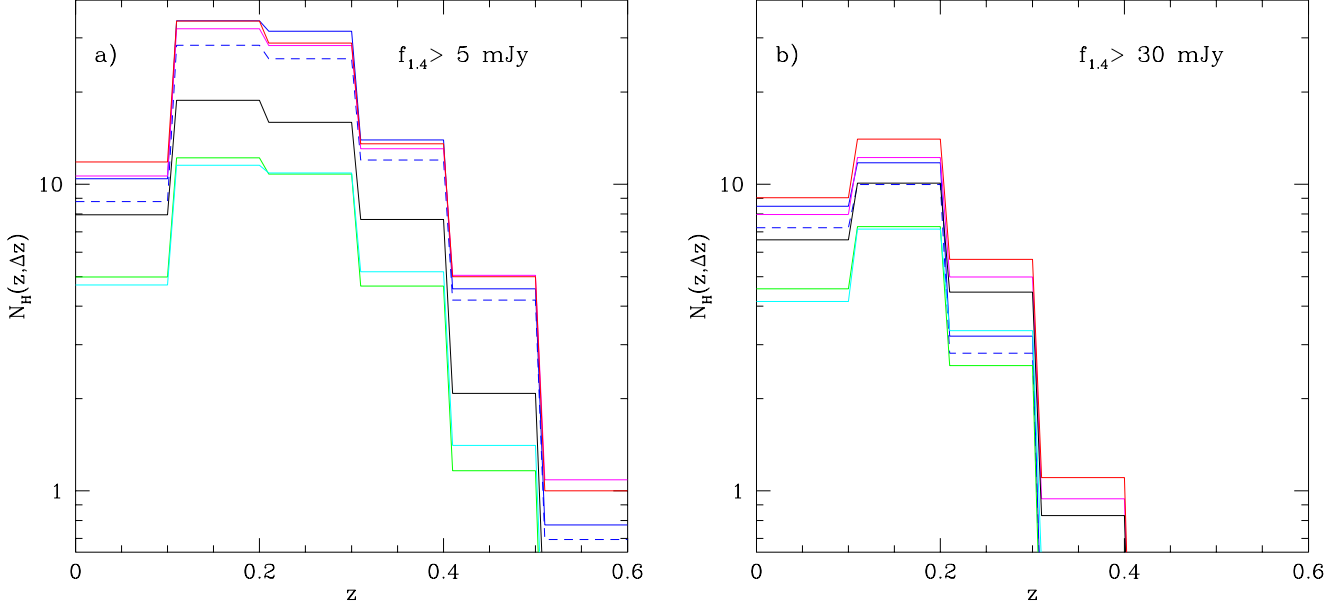


Figure 16. Expected total number of GRHs above a given radio flux in different redshift bins: panel a) above 5 mJy; panel b) above 30 mJy. In both panels the colour code is the same of Fig.11.

at $z \lesssim 0.2$ does not imply that they should also be consistent with the observed flux distribution of GRHs in the same redshift interval.

Given the RHLFs ($dN_H(z)/dP_{1.4}dV$) the number of GRHs with $f > f_{1.4}$ is given by:

$$N_H(> f_{1.4}) = \int_{z=0}^z dz' \left(\frac{dV}{dz'} \right) \int_{P_{1.4}(f_{1.4}^*, z')} \frac{dN_H(P_{1.4}, z')}{dP_{1.4} dV} dP_{1.4} (20)$$

where dV/dz is the comoving volume element in the Λ CDM cosmology (e.g., Carroll, Press and Turner 1992); the radio flux and the radio power are related by $P_{1.4} = 4\pi d_L^2 f_{1.4}$ with d_L the luminosity distance (where we neglect the K-correction since the slope of the spectrum of radio halos is close to unity).

As a first step, we use Eq. 20 to calculate the number of expected GRHs above a given radio flux at 1.4 GHz from a full sky coverage up to $z \lesssim 0.2$ and compare the results with number counts derived by making use of the present day observations (Fig. 14, the colour code is that of Fig.11). Calculations in Fig. 14 are obtained by using the full bundle of RHLFs obtained in the previous Section (Fig. 13). The black points are obtained by making use of the radio data from the analysis of the radio survey NVSS by Giovannini et al.(1999); normalization of counts is scaled to correct for the incompleteness due to the sky-coverage in Giovannini et al. ($\sim 2\pi$ sr). The NVSS has a 1σ level at 1.4 GHz equal to 0.45 mJy/beam (beam= 45×45 arcsec, Condon et al. 1998). By adopting a typical size of GRH of the order of 1 Mpc, the surface brightness of the objects which populate the peak of the RHLFs ($\sim 10^{24}$ W/Hz) at $z \sim 0.15$ is expected to fall below the 2σ limit of the NVSS. These GRHs have a flux of about 20 mJy, thus below this flux the NVSS becomes poorly efficient in catching the bulk of GRHs in the redshift bin $z=0-0.2$ and a fair comparison with observations is not possible. For larger fluxes we find that the expected number

counts are in excellent agreement with the counts obtained from the observations. We note that assuming a superlinear scaling of B with cluster mass, up to 30-40 GRHs at $z < 0.2$ are expected to be discovered with future deeper radio surveys. On the other hand, the number of these GRHs in the case of a sublinear scaling should only be a factor of ~ 2 larger than that of presently known halos.

As a second step, we calculate (Fig.15) the whole sky number of GRHs expected up to $z = 0.7$ (the probability to form GRHs at $z > 0.7$ is negligible). We note that the number counts of GRHs increases down to a radio flux

of $f_{1.4} \sim 2 - 3$ mJy and then flattens due to the strong (negative) evolution of the RHLFs (Fig. 13). We note that the expected total number of GRHs above 1 mJy at 1.4 GHz is of the order of ~ 100 depending on the scaling of the magnetic field with cluster mass.

Finally we calculate the expected number counts of GRHs above a given radio flux in different redshift bins. This allows us to catch the redshift at which the bulk of GRHs is expected. In Fig. 16 we report the RHNCs integrated above 5 mJy (Panel a)) and above 30 mJy (Panel b)). We note that the bulk of GRHs is expected in the redshift interval $0.1 - 0.3$ and this does not strongly depend on the flux limit. We note that the relatively high value of such redshift range is also due to the presence of the low radio power cut-off in the RHLFs which suppresses the expected number of low power GRHs. On the other hand, at radio fluxes > 30 mJy the contribution from higher redshift decreases since the requested radio luminosities at these redshift correspond to masses of the parent clusters which are above the high-mass cut-off of the cluster mass function.

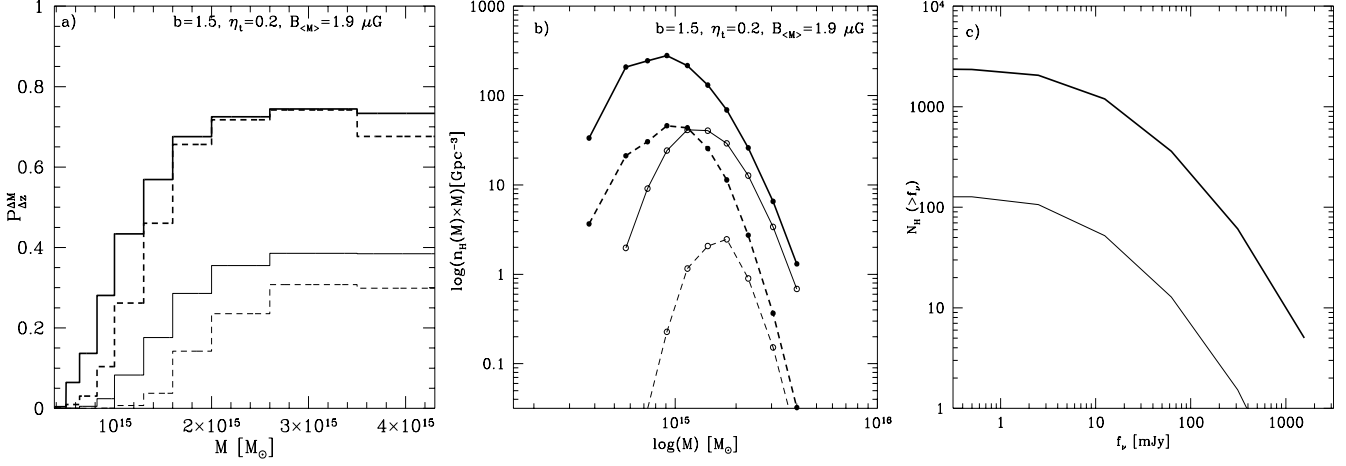


Figure 17. **a)** The occurrences of GRHs as a function of the cluster mass in the redshift bins 0-0.1 (solid lines) and 0.4-0.5 (dashed lines) are reported for 150 MHz (thick lines) and for 1.4 GHz (thin lines). **b)** Mass functions of GRHs in the redshift bins 0-0.1 (solid lines) and 0.4-0.5 (dashed lines) are reported for 150 MHz (thick lines) and for 1.4 GHz (thin lines). **c)** Comparison between the expected RHNCs above a given radio flux at 1.4 GHz (thin lines) and at 150 MHz (thick lines) from a full sky coverage up to $z \leq 0.6$. All the calculations have been performed assuming: $b=1.5$, $B_{<M>} = 1.9\mu\text{G}$ and $\eta_t = 0.2$.

7 TOWARDS LOW RADIO FREQUENCIES: MODEL EXPECTATIONS AT 150 MHz

Due to their steep radio-spectra, GRHs are ideal targets for upcoming low-frequency radio telescopes, such as LOFAR and LWA. In this section we present calculations of the statistics of GRHs at 150 MHz derived from the electron reacceleration model.

For simplicity, we present these results only for one set of the parameters in the plane $(B_{<M>}, b)$ (Fig.7): a super-linear case ($b=1.5$, $B_{<M>} = 1.9\mu\text{G}$) (see Sec.3).

First, we calculate the probability to have GRHs at ~ 150 MHz as a function of the cluster's mass following the procedure outlined in Sec.4.1 and requiring a break frequency $\nu_b \gtrsim 20$ MHz to account for the observation frequency. In Fig.17a we report the probability to have GRHs as a function of virial mass in two redshift bins at 1.4 GHz (thin lines) and at 150 MHz (thick lines). As expected, the probability at 150 MHz is substantially larger than that calculated at 1.4 GHz, particularly for higher redshifts and for low massive clusters.

One of the main findings of our work is the presence of a cut-off in the RHLFs at low radio powers (see Sec.5), which reflects the drop of the probability to form GRHs as the cluster's mass decreases. In Fig.17b we plot the mass functions of radio halos (RHMFs) at 1.4 GHz and at 150 MHz in two redshift bins (see caption of Fig.17). We note that the number density of GRHs is increased by only a factor ~ 2 for $M > 2 \cdot 10^{15} M_\odot$, but by more than one order of magnitude for $M \leq 10^{15} M_\odot$. The most interesting feature is again the presence of a low mass cut-off in the RHMFs at 150 MHz, which however is shifted by a factor ~ 2 towards smaller masses with respect to the case at 1.4 GHz. This is related to the fact that a smaller energy density in the form of turbulence is sufficient to boost GRHs at lower frequencies, and this allows the formation of GRHs also in slightly smaller clusters, which indeed are expected to be less turbulent (CB05; see also Vazza et al. 2006).

Finally, in order to obtain estimates for the RHLFs and

RHNCs at 150 MHz, we tentatively assume the same $P_R - M$ scaling found at 1.4 GHz, scaled at 150 MHz with an average spectral index $\alpha_\nu \sim 1.2$, and follow the approach outlined in Secs. 5 and 6. In Fig.17c we report the expected integral number counts of radio halos from a full sky coverage above a given radio flux at 1.4 GHz (thin lines) and at 150 MHz (thick lines) up to a redshift $z \sim 0.6$. The expected number of GRHs at 150 MHz are a factor of ~ 10 larger than the number expected at 1.4 GHz, with the bulk of GRHs at fluxes \geq few mJy. In the near future LOFAR will be able to detect diffuse emission on Mpc scale at 150 MHz down to these fluxes and this would be sufficient to catch the bulk of these GRHs (a more detailed study will be presented in a forthcoming paper).

8 SUMMARY AND DISCUSSION

The observed correlations between radio and X-ray properties of galaxy clusters provide useful tools to constraining the physical parameters that are relevant to the reacceleration models for the onset of giant radio halos (GRHs). Our analysis is based on the calculations of Cassano & Brunetti (2005; CB05), which assumes that a seed population of relativistic electrons reaccelerated by magnetosonic (MS) waves is released in the ICM by relatively recent merger events. To this end we have collected from the literature a sample of 17 GRH clusters for all of which, but one (A2254), both radio and X-ray homogeneous data are available, as summarized in Tab.1 & 2. Based on the relationships derived in CB05 paper, we have been able to constrain the (likely) dependence of the average magnetic field intensity (B) on the cluster mass, under the assumption that B can be parameterized as $B = B_{<M>}(M / \langle M \rangle)^b$ (with $B_{<M>}$ the average field intensity of a cluster of mean mass $\langle M \rangle = 1.6 \times 10^{15} M_\odot$ and b positive). This is an important achievement because both the emitted synchrotron spectrum and losses depend critically on the field intensity. Following CB05 approach, the merger events are obtained in the statistical scenario

provided by the extended Press & Schechter formalism that describes the hierarchical formation of galaxy clusters. The main results of our study can be summarized as follows:

- *Observed correlations*

In Sect.2 we derive the correlations between the radio power at 1.4 GHz ($P_{1.4}$) and the X-ray luminosity (0.1–2.4 keV), ICM temperature and cluster mass. Most important for the purpose of the present investigation is the $P_{1.4} - M_v$ correlation which has been derived by combining the $L_X - M_v$ correlation obtained for a large statistical sample of galaxy clusters (the HIFLUGCS sample plus our sample) with the $P_{1.4} - L_X$ correlation derived for our sample of GRHs. This procedure allows us to avoid the well known uncertainties and limits which are introduced in measuring the masses of small samples of galaxy clusters, especially in the case of merging systems. We find a value of the slope $\alpha_M = 2.9 \pm 0.4$ ($P_{1.4} \propto M_v^{\alpha_M}$). A steep correlation of the synchrotron luminosity with the ICM temperature is also found, although with a large statistical error in the determination of the slope: $\alpha_T = 6.4 \pm 1.6$ ($P_{1.4} \propto T^{\alpha_T}$).

In Sec.2 we have also shown that at least in the case of high X-ray luminosity clusters ($L_X \gtrsim 5 \cdot 10^{44}$ erg/s) the above trends are unlikely driven by selection effects in the present observations.

- *Constraining the magnetic field dependence on the mass*

A correlation between the radio power and the cluster virial mass is naturally expected in the framework of electron acceleration models. This relationship, discussed in Sec. 3.1 (Eq.12), can reproduce the observed correlation for viable values of the physical parameters. For instance, in the case $B \ll B_{cmb}$, it is $P(\nu_o) \propto M_v^{a(2-\Gamma+b)+b}$ and the exponent agrees with the observed one ($\alpha_M \sim 3$) by adopting a typical slope of the radio spectrum $a = 1 - 1.2$ and a sub-linear scaling $b \sim 0.6 - 0.8$.

A systematic comparison of the expected correlations between the radio power and the cluster mass with the observed one (Sect.3.1 & 2) allows the definition of a permitted region of the parameters' space ($B_{<M>}, b$), where a lower bound $B_{<M>} = 0.2 \mu\text{G}$ is obtained in order not to overproduce via the IC scattering of the CMB photons the hard X-ray fluxes observed in the direction of a few GRHs (Sect. 3.3 and Fig.6). It is found a lower bound at $b \sim 0.5 - 0.6$ and that a relatively narrow range of $B_{<M>}$ values is allowed for a fixed b . The boundaries of the allowed region, aside from the lower bound of $B_{<M>}$, are essentially sensitive to the limits from the $P_{1.4} - M_v$ correlation.

A super-linear scaling of B with mass, as expected by MHD simulations (Dolag et al. 2004) falls within the allowed region.

The values of the average magnetic field intensity in the superlinear case are close (slightly smaller) to those obtained from the Faraday rotation measurements (e.g., Govoni & Feretti 2004), which, however, generally sample regions which are even more internally placed than those spanned by GRHs.

Future observations will allow to better constrain the radio-X ray correlations and thus to better define the region

of the model parameters.

- *Probability to form GRHs*

In Sect.4 we report on extensive calculations aimed at constraining η_t , the fraction of the available energy in MS waves, which is required to match the observed occurrence of GRHs at redshifts $z \leq 0.2$ (Fig.7). By adopting a representative sampling of the allowed ($B_{<M>}, b$) parameter space (Fig.6) we find $0.15 \leq \eta_t \leq 0.44$: the larger values are obtained for $B_{<M>}$ approaching the lower bound of the allowed region, because of the larger acceleration efficiency necessary to boost electrons at higher energies to obtain a fixed fraction of clusters with GRHs.

With an appropriate η_t value for each set of ($B_{<M>}, b$) parameters we can calculate the probability of occurrence of GRHs at larger redshifts for which observational data are not available. This probability depends on the merging history of clusters and on the relative importance of the synchrotron and IC losses, and shows a somewhat complicated behavior with cluster mass and redshift. The maximum value of this probability at a given redshift is found for a cluster mass M_* (Eq.17) which mark the transition between the Compton and the synchrotron dominated phases. In the case of sublinear scaling of the magnetic field with cluster mass ($b \sim 0.6 - 0.9$) the allowed values of the strength of the magnetic field are relatively small (Fig. 7), the value of M_* is large and the IC losses are always dominant for the mass range of clusters with known GRHs. As a consequence the probability to have GRHs increases with cluster mass and decreases with redshift (Fig 10). On the other hand superlinear scalings ($b \sim 1.2 - 1.7$) imply allowed values of $B_{<M>}$ relatively large (Fig. 7), and even larger values of the magnetic field for the most massive objects. In this case the value M_* falls within the range of masses spanned by GRH clusters: the predicted fraction of clusters with GRHs increases with mass, then reaches a maximum value at about $M_v \sim M_*$, and finally falls down for larger masses (Fig 9). At variance with the case of sublinear scaling, in this case the fraction of the most massive objects with GRHs is expected to slightly increase with redshift, at least up to $z=0.2-0.4$ (Fig 9) where the bulk of turbulence is injected in a Λ CDM model (CB05).

- *Luminosity functions (RHLFs)*

In Sect.5 we report the results of extensive calculations following a fair sampling of the ($B_{<M>}, b$) allowed region as summarized in Tab. 3; this essentially allows a full coverage of all possible RHLFs given the present correlations at 1σ . We find that, although the large uncertainties in the ($B_{<M>}, b$) region, the predicted local RHLFs are confined to a rather narrow bundle, the most characteristic common feature being the presence of a flattening/cut-off at radio powers below about 10^{24} W/Hz at 1.4 GHz (Fig.11). The fraction of GRHs with 1.4 GHz luminosity below $\sim 5 \times 10^{22}$ W $\text{Hz}^{-1} h_{70}^{-2}$, a factor of ~ 5 smaller than the luminosity of the less powerful GRH (A2256, $z=0.0581$) known so far, is negligible. This characteristic shape of the RHLFs, obtained in our paper for the first time, represents a unique prediction of particle acceleration models, and does not depend on the adopted physical details for the particle acceleration mecha-

nism. This is due to the decrease of the efficiency of particle acceleration in the case of less massive clusters which is related to three major reasons (see CB05):

- i) smaller clusters are less turbulent than larger ones since the turbulent energy is expected to scale with the thermal one (CB05; see also Vazza et al. 2006);
- ii) turbulence is typically injected in large Mpc regions in more massive clusters and thus these are favoured for the formation of GRHs (CB05);
- iii) since in the present paper we found $B \propto M^b$ with $b \gtrsim 0.5$, higher energy electrons should be accelerated in smaller clusters to emit synchrotron radiation at a given frequency.

Deep radio survey with future radio telescopes (LOFAR, LWA, SKA) are required to test the presence of this cut-off/flattening in the luminosity function of the GRHs.

The predicted evolution of the RHLFs with redshift is illustrated in Fig. 13: the comoving number density of GRHs decreases with redshift due to the evolutions of the cluster mass function and of the probability to form GRHs. The decrease with redshift of the RHLFs calculated by adopting sublinear scaling of the magnetic field with cluster mass is faster than that in the superlinear scaling causing a spread in the RHLFs bundle with z .

• Number counts (RHNCs)

In Sec.7 we have derived the integral number counts of GRHs at 1.4 GHz. We find that the number counts predicted for the same set of RHLFs discussed in Secs.6 generally agree with those derived from the NVSS at the limit of this survey and within $z = 0.2$ (Fig.14). The flattening of the counts below $\sim 50 - 60$ mJy is both due to the combination of the low power cut-offs of the RHLFs with the redshift limit, and to the RHLFs evolution with redshift. On the other hand, past calculations which assume a fixed fraction of GRHs with cluster mass predict an increasing number of sources at lower fluxes (e.g., Enßlin & Röttgering, 2002).

GRHs around the peak of our LFs ($P_{1.4GHz} \sim 10^{24}$ W/Hz) and at $z \sim 0.15$ would be detectable at fluxes below about 20 mJy, which however is below the sensitivity limit of the NVSS for this type of objects. We estimate that the number of GRHs below this flux could be up to 30-40 (whole sky, $z \leq 0.2$) if superlinear scalings of the mass with B hold.

The predicted number of GRHs (Fig.15) (whole Universe) could be up to $\gtrsim 100$ if a superlinear scaling of the mass with B holds, while a sublinear scaling would give a number 2-3 times smaller. A substantial number of these objects would be found also down to a flux of a few mJy at 1.4 GHz in the case of a superlinear scaling, while in the case of sublinear scalings the number of GRHs below about 10 mJy would be negligible.

We also find that the bulk of GRHs is expected at $z \sim 0.1-0.3$ (Fig.16). It should be mainly composed by those RHs populating the peak of the RHLFs, i.e. objects similar (or slightly more powerful) to the GRH in the Coma cluster.

• Toward expectations at low radio frequencies

In Sec.7 we have extended our estimates to the case of low frequency observations which will be made with upcom-

ing instruments, such as LOFAR and LWA. Lower energetic electrons contribute to these frequencies and thus - in the framework of the particle re-acceleration scenario - the efficiency of producing GRHs in galaxy clusters is expected to be higher than that of GRHs emitting at 1.4 GHz.

By presenting the analysis for a representative set of parameters, we have shown that the probability to have GRHs emitting at 150 MHz is significantly larger than that of those emitting at 1.4 GHz, particularly in the mass range $\sim 5 \cdot 10^{14} - 1.5 \cdot 10^{15} M_{\odot}$. Consequently, the low mass cut-off in the RHMFs is shifted down by a factor of ~ 2 . This is naturally expected and is due to the fact that slightly less turbulent systems are able to generate GRHs at lower frequencies.

We have also estimated that the number counts of GRHs at low frequencies might outnumber those at 1.4 GHz by at least one order of magnitude. We venture to predict that LOFAR is likely to discover $\gtrsim 10^3$ (all sky) GRHs down to a flux of few mJy at 150 MHz.

ACKNOWLEDGMENTS

RC warmly thank S.Ettori and C.Lari for useful discussions on the statistical analysis. We acknowledge D.Dallacasa, K.Dolag and L.Feretti for comments on the manuscript, and T.Ensslin for useful discussions and for kindly providing the Local RHLFs in Fig. 11. The anonymous referee is acknowledged for useful comments. RC acknowledge the MPA in Garching for the hospitality during the preparation of this paper. This work is partially supported by MIUR under grant PRIN2004.

REFERENCES

- Akritas M.G., Bershadsky M.A., 1996, ApJ 470, 706
- Bacchi M., Feretti L., Giovannini G., Govoni F., 2003, A&A 400, 465
- Bertoglio J.-P., Bataille F., Marion J.-D., 2001, Physics of Fluids 13, 290
- Berezinsky V.S., Blasi P., Ptuskin V.S., 1997, ApJ 487, 529
- Böhringer H., Schuecker P., Guzzo L., Collins C. A., Voges W., Cruddace R. G., Ortiz-Gil A., Chincarini G., De Grandi S., Edge A. C., and 4 coauthors, 2004, A&A 425, 367
- Blasi P., 2004, JKAS 37, 483.
- Bowyer S., Korpela E.J., Lampton M., Jones T.W., 2004, ApJ 605, 168.
- Brunetti G., 2003, in 'Matter and Energy in Clusters of Galaxies', ASP Conf. Series, vol.301, p.349, eds. S. Bowyer and C.-Y. Hwang
- Brunetti G., 2004, JKAS 37, 493
- Brunetti G., 2006, Astronomische Nachrichten 327, No 5/6, 615 (proceedings of "The Origin and Evolution of Cosmic Magnetism", 29 August - 2 September 2005, Bologna, Italy)
- Brunetti G., Setti G., Feretti L., Giovannini G., 2001, MNRAS 320, 365
- Brunetti G., Blasi P., Cassano R., Gabici S., 2004, MNRAS 350, 1174
- Brunetti G., Blasi P., 2005, MNRAS 363, 1173
- Buote D.A., 2001, ApJ 553, 15
- Carroll S.M., Press W.H., Turner E.L., 1992, ARA&A 30, 499
- Cassano R. & Brunetti G., 2005, MNRAS 357, 1313
- Colafrancesco S., 1999, in "Diffuse thermal and relativistic plasma in galaxy clusters". Edited by Böhringer H., Feretti L.,

- Schuecker P., Garching, Germany : Max-Planck-Institut für Extraterrestrische Physik, 1999. ("Proceedings of the Workshop...Ringberg Castle, Germany, April 19-23, 1999".), p.269
- Colafrancesco S., Marchegiani P., Perola G.C., 2005b, *A&A* in press, astro-ph/0506565
- Condon J.J., Cotton W.D., Greisen E.W., Yin Q.F., Perley R.A., Taylor G.B., Broderick J.J., 1998, *AJ* 115, 1693
- David L. P., Slyz A., Jones C., Forman W., Vrtillek S. D., Arnaud K. A., 1993, *ApJ* 412, 479
- Dennison B., 1980, *ApJ* 239
- Deiss B.M., Reich W., Lesch H., Wielebinski R., 1997 *A&A* 321, 55
- Dolag K., 2006, invited review, *Astronomische Nachrichten* in press (proceedings of "The Origin and Evolution of Cosmic Magnetism", 29 August - 2 September 2005, Bologna, Italy), astro-ph/0601484
- Dolag K., Bartelmann M., Lesch H., 2002, *A&A* 387, 383
- Dolag K., Grasso D., Springel V., Tkachev I., 2004, *JKAS* 37, 427
- Ebeling H., Voges W., Bohringer H., Edge A. C., Huchra J. P., Briel U. G., 1996, *MNRAS* 281, 799
- Ebeling H., Edge A. C., Bohringer H., Allen S. W., Crawford C. S., Fabian A. C., Voges W., Huchra J. P., 1998, *MNRAS* 301, 881
- Enßlin T.A., 2004, *JKAS* 37, 439
- Enßlin T.A., Biermann P.L.; Kronberg P.P., Wu X.-P., 1997, *ApJ* 477, 560
- Enßlin T.A., Biermann P.L., Klein U.; Kohle S., 1998, *A&A* 332, 395
- Enßlin T.A., Gopal-Krishna, 2001, *A&A* 366, 26
- Enßlin T.A., Röttgering H., 2002, *A&A*, 396, 83
- Evrard A.E., Metzler C.A., Navarro J.F., 1996, *ApJ* 469, 494
- Ettori S., Fabian A.C., 1999, *MNRAS* 305, 834
- Ettori S., Tozzi P., Borgani S., Rosati P., 2004 *A&A* 417, 13
- Feretti L., 2000, Invited review at IAU 199 'The Universe at Low Radio Frequencies' in Pune, India, 1999
- Feretti L., 2002, in "The Universe at Low Radio Frequencies", Proceedings of IAU Symposium 199, held 30 Nov - 4 Dec 1999, Pune, India. Edited by A. Pramesh Rao, G. Swarup, and Gopal-Krishna, p.133
- Feretti L., 2003, in "Matter and Energy in Clusters of Galaxies", ASP Conf. Series, vol.301, p.143, eds. S. Bowyer and C.-Y. Hwang.
- Feretti L., 2004, in "X-Ray and Radio Connections", eds. L.O. Sjouwerman and K.K. Dyer, published electronically by NRAO, Held 3-6 February 2004 in Santa Fe, New Mexico, USA.
- Feretti L., Fusco-Femiano R., Giovannini G., Govoni F., 2001, *A&A* 373, 106
- Feretti L., Brunetti G., Giovannini G., Kassim N., Orrú E., Setti G., 2004, *JKAS* 37, 315
- Feretti L., Orrú E., Brunetti G., Giovannini G., Kassim N., Setti G., 2004, *A&A* 423, 111
- Fusco-Femiano R., Dal Fiume D., Orlandini M., De Grandi S., Molendi S., Feretti L., Grandi P., Giovannini G., 2003, in 'Matter and Energy in Clusters of Galaxies', ASP Conf. Series, eds., vol.301, p.109, S. Bowyer and C.-Y. Hwang
- Fusco-Femiano R., Orlandini M., Brunetti G., Feretti L., Giovannini G., Grandi P., Setti G., 2004, *ApJ* 602, 73
- Fujita Y., Takizawa M., Sarazin C.L., 2003, *ApJ* 584, 190
- Gabici S., Balsi P., 2003, *ApJ* 583, 695
- Giovannini G., Tordi M., Feretti L., 1999, *NewA* 4, 141
- Giovannini G., Feretti L., 2000, *NewA* 5, 335
- Giovannini G., Feretti L., 2002 in 'Merging Processes in Galaxy Cluster', vol.272, p.197, eds. L.Feretti, I.M.Gioia, G.Giovannini
- Govoni F., Feretti L., Giovannini G., Böhringer H., Reiprich T.H., Murgia M., 2001, *A&A*, 376, 803
- Govoni F., Markevitch M., Vikhlinin A., VanSpeybroeck L., Feretti, L., Giovannini G., 2004, *ApJ* 605, 695
- Govoni F., Feretti L., 2004, *Int. J. Mod. Phys. D* 13, 1549
- Govoni F., Murgia M., Feretti L., Giovannini G., Dallacasa D., Taylor G. B., 2005, *A&A* 430, 5
- Hwang C.-Y., 2004, *JKAS* 37, 461
- Hoefl M., Brggen M.; Yepes G., 2004, *MNRAS* 347, 389
- Hogg D.W., 2000, astro-ph/9905116
- Hughes J.P., Butcher J.A., Stewart G.C., Tanaka Y., 1993, *ApJ* 404, 611
- Kaastra J.S., Lieu R., Tamura T., Paerels F.B.S., den Herder J.W., 2003, *A&A* 397, 445
- Kempner J.C., Sarazin C.L., 2001, *ApJ* 548, 639
- Kim K.-T., Kronberg P.P., Dewdney P.E., Landecker T.L., 1990, *ApJ* 355, 29
- Kitayama T., Suto Y., 1996, *ApJ* 469, 480
- Kuo P.-H., Hwang C.-Y., Ip W.-H., 2004, *ApJ* 604, 108
- Kuo P.-H., Hwang C.-Y.; Ip, W.-H., 2003, *ApJ* 594, 732
- Lacey, C., Cole S., 1993, *MNRAS* 262, 627
- Lazarian A., 2006, invited review, *Astronomische Nachrichten* in press (proceedings of "The Origin and Evolution of Cosmic Magnetism", 29 August - 2 September 2005, Bologna, Italy)
- Lemonon L., Pierre M., Hunstead R., Reid A., Mellier Y., Böhringer H., 1997, *A&A* 326, 34
- Liang H., 1999, in "Diffuse thermal and relativistic plasma in galaxy clusters". Edited by Bohringer H., Feretti L., Schuecker P., Garching, Germany : Max-Planck-Institut für Extraterrestrische Physik, 1999. ("Proceedings of the Workshop...Ringberg Castle, Germany, April 19-23, 1999".), p.33
- Liang H., Hunstead R.W., Birkinshaw M., Andreani P., 2000, *ApJ* 544, 686
- Markevitch M., 1996, *ApJ*, 465, 1
- Markevitch M., Forman W. R., Sarazin C. L., Vikhlinin A., 1998, *ApJ* 503, 77
- Markevitch M., Gonzalez A.H., David L., Vikhlinin A., Murray S., Forman W., Jones C., Tucker W., 2002, *ApJ* 567, 27
- Miniati F., Jones T.W., Kang H., Ryu D., 2001, *ApJ* 562, 233
- Mushotzky R. F., Scharf C. A., 1997, *ApJ* 482, 13
- Nevalainen J., Markevitch M., Forman W., 2000, *ApJ* 532, 694
- Petrosian V., 2001, *ApJ* 557, 560
- Pfrommer C., Enßlin T.A., 2004, *A&A* 413, 17
- Pierre M., Matsumoto H., Tsuru T., Ebeling H., Hunstead R., 1999, *A&AS* 136, 173
- Press W.H., Schechter P., 1974, *ApJ* 187, 425
- Rephaeli Y., Gruber D., 2003, *ApJ* 595, 137
- Reimer O., Pohl M., Sreekumar P., Mattox J.R., 2003, *ApJ* 588, 155
- Reimer A., Reimer O., Schlickeiser R., Iyudin A., 2004, *A&A* 424, 773
- Reiprich T.H., Böhringer H., 2002, *ApJ* 567, 716
- Roettiger K., Burns J.O., Loken C., 1996, *ApJ* 473, 651
- Roettiger K., Burns J.O., Stone J.M., 1999, *ApJ* 518, 603
- Ryu D., Kang H., Hallman E., Jones T.W., 2003, *ApJ* 593, 599
- Sarazin C.L., 1986, *Reviews of Modern Physics* 58, 1
- Sarazin C.L., 1999, *ApJ* 520, 529
- Sarazin C.L., 2002, in 'Merging Processes in Clusters of Galaxies', vol.272, p.1, edited by L. Feretti, I. M. Gioia, and G. Giovannini
- Schindler S., 1996, *A&A* 305, 756
- Schindler S., 2002, in "Merging Processes in Galaxy Clusters." Edited by L. Feretti, I.M. Gioia, G. Giovannini. Astrophysics and Space Science Library, Vol. 272. Kluwer Academic Publishers, Dordrecht, 2002, p. 229-251
- Schuecker P., Böhringer H.; Reiprich T.H., Feretti L., 2001, *A&A* 378, 408
- Schlickeiser R., Sievers A., Thiemann H., 1987, *A&A* 182, 21
- Tsuru T., Koyama K., Hughes J.P., Arimito N., Kii T., Hattori M., 1996, in "UV and X-ray Spectroscopy of Astrophysical and Laboratory Plasmas": Edited by K. Yamashita and T.

- Watanabe. Tokyo : Universal Academy Press, 1996. (Frontiers science series ; no. 15)., p.375
- Vazza F., Tormen G., Cassano R., Brunetti G., Dolag K., 2006, accepted for publication in MNRAS Letters, astro-ph/0602247
- Venturi T., Bardelli S., Dallacasa D., Brunetti G., Giacintucci S., Hunstead R.W., Morganti R., 2003, A&A 402, 913
- Völk H.J., Aharonian F.A., Breitschwerdt D., 1996, SSRv 75, 279
- White D. A., 2000, MNRAS 312, 663
- Zhang Y.-Y., Finoguenov A., Bhringer H., Ikebe Y., Matsushita K., Schuecker P., 2004, A&A 413, 49